POLITECNICO DI TORINO

Master's Degree in Mechanical Engineering

Master's Degree Thesis

Mechanical Properties of a Soft TPMS Cellular Metamaterial for Anatomic Applications

Supervisors

Prof. GIORGIO CHIANDUSSI

Ing. ANDREA TRIDELLO

Candidate

CARLO MICHELI

2021

Abstract

Cellular structures, also called Lattices, are structures composed by the periodic repetition of a basic minimal unit called "unit cell" in the space. This unit cell consists of a geometric structure, partially empty, which can be composed of beams, trusses or solids generated by analytic equations. Triply Periodic Minimal Surfaces are a class of periodic surfaces generated from trigonometric functions. When the sheet surface is thickened, the resulting porous geometry exhibits interesting properties, such as low density and good mechanical strength. Moreover, it is possible to tune the mechanical properties by modifying the parameters of the geometry, thanks to a modern approach to design called Field Driven Design. This ability to architect the material properties, combined with the versatility of additive manufacturing, may prove very useful in industrial and medical uses where precise structural and geometrical characteristics are required. The focus of this work was to investigate the stiffness and the crushing behaviour of some sheet-based TPMS structures manufactured with an elastomeric polymer (TPU 95A), characterized by low-stiffness and large elastic strains. The experimental results were compared to the results obtained analytically and through Finite Element simulations, showing a good correlation. The knowledge obtained was used to design and manufacture a therapeutic insole customized on the patient, using data coming from 3d-scans of the foot and baropodometric analysis (pressure distribution of the foot on the ground) to tune the lattice geometry and obtain the required mechanical properties and the most accurate shape. The procedures and the techniques used in the design and fabrication stage were explained both practically and theoretically. To conclude, the proposed methodology allows to design a product tailored around the patient need and to minimize both the manual work and the number of materials, leading to further investigations.

Dedicated to my family, who supported me during this journey.

Table of Contents

Chapter 1

Theoretical Background

Before proceeding with the core of the work and theory around lattice materials, it is important to present some of the techniques and the underlying theories. This chapter will introduce the basics of polymeric and elastomeric materials, outlining the main testing procedures and analyzing the technologies implemented, such as Additive Manufacturing and Finite Elements Analysis.

1.1 Polymeric Materials

Polymeric materials are organic substances generally obtained by chemical reactions of carbon, gas and petroleum derivatives. Their are comprised of macromolecules which are tangled together by mechanical or chemical bonds. The intermolecular forces can be weak as WanDerWaals, where an increase of temperature provides sufficient energy to loosen the bonds (thermoplastics), or strong such as covalent where the material undergoes a general degradation before melting (thermosets). The differences in chemical structure, molecular weight, frequency of intermolecular bonds, tacticity and other microscopic characteristics strongly influences the thermal and mechanical properties of the material.

Thermoplastics are often made of linear chains packed randomly in an amorphous structure: well-known examples are polyethilene (PE), polystyrene (PS) and polymethylmetacrilate (PMMA). Other times are more organized and packed regularly, which causes an increase in density, hardness and chemical resistance. Above the *glass temperature*, the weak bonds loosen and the material becomes plastic and viscous.

Thermosets are usually cross-linked with strong C-C bonds to form a compact and rigid network. The density is usually higher than thermoplastics with superior mechanical properties and they are suitable for high-temperature applications. Examples are Epoxy resins (EP) and Polyurethane (MPU).

A third class in *elastomers*, also called rubbers. They are made of long linear chain polymers with sparse connections between the chains. The glass temperature of elastomeric materials is below room temperature and without weak bonds chains can slide, only held by intermolecular covalent bonds. The scarcity of this reticulation allows for big elastic deformations (also $> 500\%$) and low rigidity[1].

1.1.1 Elastic Properties of Polymers

Polymers show three ranges of mechanical properties which depend on the temperature: the glassy regime, the transition regime and the rubber regime. The glass regime occurs at the lowest range of temperatures, where the van der Waals bonds create a higher Young's Modulus of the material, usually around 3GPa. When the temperature increases at around T_g, called *Glass Temperature*, the van der Waals bonds between molecules weaken due to thermal energy and small relative movements between chains start to be allowed, with various relaxation phenomena as the temperature increases. At temperatures around $[1.1 - 1.4]$ T_g the polymer enters the rubber regime, where the stiffness is particularly low and great strains are allowed.

For *elastomers*, polymers where cross-links between chains are placed in widely-spaced points along their lengths, the rubber regime spans over a greater range of temperatures that usually coincide with room temperature.

Above this range of temperature the thermoplastic polymers melt to a viscous flow of polymeric chains. On the contrary, thermosets with covalent carbon bonds between chains reach a temperature so high that the material degrades and burns before melting. Other types of cross-chains bonds increase the span of rubber regime without losing a proper melting temperature: TPU is an example.

1.1.2 TPU

ThermoPlastic Polyurethane is a class of Polyurethane Polymers composed by block co-polymers, which are aggregates of chains (hard and soft) bonded mechanically together. This composition of macro-blocks allows to melt the material and still retain the highly elastomeric and wear resistance properties of the polyurethane structures. The chemical composition (and thus the name) is comprised by urethane group, which is composed of ester function ($R1 - COO - R2$) and amide function ($R - CONH_2$).

The material can reach high strains with good chemical resistance (es. oils) and abrasion and wear resistance. Moreover, changing the composition of the base chains the material can be tuned to the desired compromise of hardness and elasticity.

Since TPU is thermoplastic it can be melted multiple times and used in Injection

TPU 95A			
Propery	**Symbol**	**Value**	**Unit/Scale**
Density	ρ	1281	kg/m^3
Young's Modulus (compression)	G	64	MPa
Poisson Ratio	ν	0.48	
Shore Hardness		95A	
Maximum Elongation		>550%	

Table 1.1: Average properties of TPU 95A.

Molding or in Fused Deposition Modelling, where it provides advantages such as good adhesion and little warping. Typical characteristics of this material (TPU95A) are listed in table 1.1.

1.2 Mechanical Testing of Materials

There are various standardized tests and methodologies to evaluate the mechanical properties of materials. Tensile, compression, 3 and 4 point bending tests are the most common to investigate the material subjects to static or quasi-static loads. Other tests investigate the high-strain behaviour or the creep behaviour. In the present work Compression and Hardness testing are briefly presented.

1.2.1 Compression Testing

Compressive Strength Testing (ASTM D 695 and ISO 604) is useful to define the the behavior of a material under a uniform compressive load and to extract a stress-strain diagram. The procedure and nomenclature for compression tests are similar to those for the tensile tes and Universal testing machines can be used.

The standard test specimen in ASTM D 695 is a cylinder 12.7 mm (½ in.) in diameter and 25.4 mm (1 in.) in height. The force of the compressive tool is increased by the downward thrust of the tool at a rate of 1.3 mm/min (0.05 in./min). The compressive strength is calculated by dividing the maximum compressive load by the original cross section of the test specimen.

For plastics that do not fail by shattering fracture, the compressive strength is an arbitrary value and not a fundamental property of the material tested. When there is no brittle failure, compressive strength is reported at a particular deformation level such as 1 or 10%. Compressive strength of plastics may be useful in comparing materials, but it is especially significant in the evaluation of cellular or foamed plastics.

Compression testing of cellular plastics is addressed in ISO Standards 1856 and 3386–1[2]. Generally, the compressive modulus and strength are higher than the corresponding tensile values for a given material.

1.2.2 Hardness Testing

Tests for measuring hardness of Polymers are Rockwell testing, *Shore durometer* and Barcol method[2]. Hardness conversion between one scale and the other depends on many factors, such as recovery and creep.

Leaving Barcol Method aside, the difference between Rockwell and Shore testing is that Rockwell is more suitable for hard and structural plastics, whereas Shore durometer allows to measure the hardness of soft plastics and rubbers.

In fact Rockwell requires to measure the difference in the size of a ball-indentation on the material surface between the application of a minor and a major load. Instead the durometer method (ISO 868, ASTM D2240) registers the amount of indentation caused by a single spring loaded pointed indenter [2]. There are various configurations of indentor size/shape and spring loads. Each of these configurations returns a value between 0 and 100 that is usually considered valid when the value is $\in$ [10,90], othewise a different cofiguration has to be adopted. Common durometer types are A and D.

Durometer type	Applications
A	Soft vulcanized rubber and all elastomeric materials, natural rubber, GR-S, GR-1, neoprene, nitrile rubbers, Thiokol, flexible polyester cast resins, polyacrylic esters, wax, felt, and leather
D	Hard rubber and the harder grades of plastics such as rigid thermoplastic sheet. Plexiglas (AtoHaas Americas Inc.), polystyrene, vinyl sheet, cellulose acetate and thermosetting laminates such as Formica (Formica Corp., Cincinnati, OH), paperfilled calendar rolls, and calendar bowls

Table 1.2: Description of suitable material samples from [3]

The test has to be performed on a sample at least 6 mm thick and the value changes depending on the measurement setting. For example, for viscoelastic material is time dependent and can be taken at a specific time step (applying load with a certain force) or at an equilibrium time. Another variable is the conditioning of the sample, because humidity and temperature levels affect the effective hardness of the material.

TPU `95A` refers to a hardness of 95 measured with a type A Shore durometer. Figure 1.1 shows a reference charts for various materials. It can be seen that 95A is positioned on the right side of the chart and thus is a quite hard material. Hardness

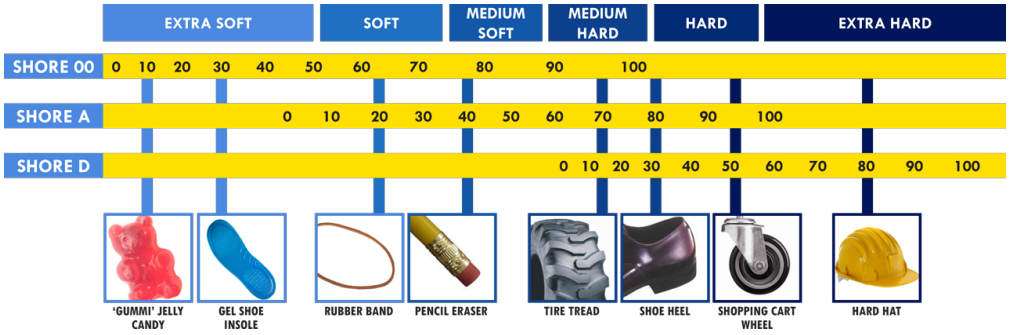

Figure 1.1: Shore hardness of common objects.

properties of a material have a direct correlation to the yield strength properties, since it measures the local plastic deformation under a load.

1.3 Field-Driven Design

Field-Driven design refers to a new approach in the Computer-Aided Design of components which relies on different foundations than traditional CAD. Most of the drawing software is based on some basic geometrical entities, such as lines, circles and primitive curves called *NURBS*. The shape of these curves is defined by some control points that control position and curvature. Surfaces are generated by connecting two or more splines together and solid bodies are defined by a collection of boundary surfaces, which define a closed region of space.

This framework of points, curves and surfaces gives the freedom to precisely draw aesthetic elements and control the surface continuity of elements (for example in industrial design applications) but has some major drawbacks.

In fact, the number of control points required grows with the geometrical complexity of the body. For example, a lattice body can be comprised of several complex surfaces and the number of element scales up as n^3, which is the cube of the component diameter. The size and complexity of the CAD file soon becomes impossible to be managed properly.

The second main disadvantage of the traditional design approach is that some operations such as fillet, offset and boolean union/difference/intersection are very prone to failure because the topology of the solid may change and new sets of curves must be extrapolated.

For such cases, a different approach to design is available. In this approach bodies are described by distance fields, positive in the outside and negative in the

inside. Null values coincides with the body boundary surface. For example a sphere of center $(x0, y0, z0)$ and radius R is defined by

$$f(x, y, z) = \sqrt{(x - x0)^2 + (y - y0)^2 + (z - z0)^2 - R^2}$$

an expression that comes from algebra. It's easy to verify that for radius $r > R$ the value of the *scalar field* f is positive (outside) and for $r < R$ is negative (inside) and is equal to the distance from the sphere surface. The solid body satisfies the inequality $f(x, y, z) < 0$, the surface of the solid body $f(x, y, z) = 0$ and is said to be an *implicit body* because is defined by implicit equations. This formulation does not require to define any complex curve or surface and it's exact, meaning that is not approximated. Similarly planes, boxes, cylinders are defined by simple equations or system of equations.

From this definition it's possible to offset a surface just by subtracting the offset thickness t_o to the implicit equation $f' = f - t_o$. In addition, the thickness may be a scalar field, function of the space just like $t_o(x, y, z)$ so variable offset is generated. To perform a boolean operation it's sufficient to analytically combine the scalar fields of two or more implicit bodies. For example the union of two implicit bodies $A = f_a(x, y, z)$ and $B = f_b(x, y, z)$ is defined as:

$$A \cup B = min(A, B) \tag{1.1}$$

where the function $min()$ takes the minimum value between the two distance fields. Similarly a boolean intersection is:

$$A \cap B = min(abs(A), abs(B)) \ \cdot \ max(sign(A), sign(B)) \tag{1.2}$$

Many other different types of operations are possible. It's even possible to deform a body by deforming it's coordinate grid (ex. $(x, y, z)' = f(x, y, z)$). Moreover this mathematical definitions is fault-proof meaning that it always provides an existing and coherent result, independently from the input fields. For the reasons presented here, field-driven design is particularly suitable for the design and optimization of lattices (insight on the topic in chapter 2).

From a practical point of view, the implementation of field driven design has been written in Matlab but there are some commercial software available, in particular *nTopology*[4] which offers built-in functions for implicit design and lattice generation. The mathematical approach to design allowed nTopology to implement a nested workflow, where each function in represented by a block. This scripting-like workflow lets the user to iterate and change parameters, running finite-element simulations and performing topology optimizations.

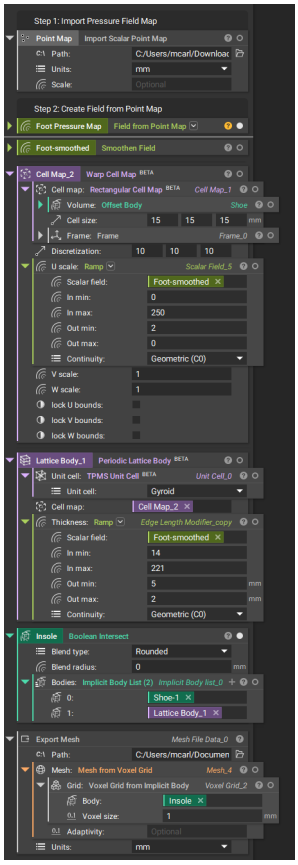

(a) nTopology workflow for generating lattice (example of chapter 4). This nested scripting-like approach to design allows to update the input data and perform complex operations on implicit geometries.

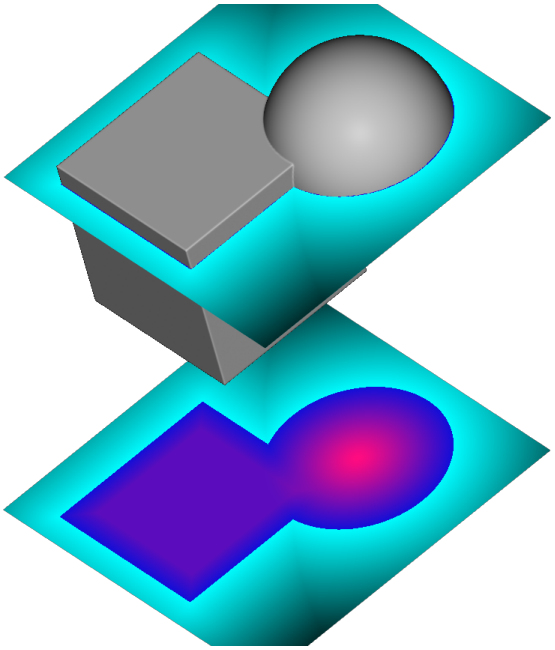

(b) Implicit field of the union between a sphere and a cube. Positive values goes from blue to black and negative values from purple to pink.

1.4 Finite Element Analysis

Finite Element is a numerical method widely used for the prediction of the response of mechanical, thermal and fluid dynamic systems. It is based on the approximation of a continuum by dividing it into geometrically simple regions of finite size, which are simple enough to have an analytical description. FE is suitable to solve problems with differential formulation. For the solution of mechanical systems, the equations describing elastic behaviour of materials are combined together. The full system includes:

- *equilibrium equations* which are needed to balance the forces and the torques. This differential equations can eventually be integrated;

- *compatibility equations* (differential) that describe deformations of the elements;
- *constitutive laws of materials* which link together forces and deformations.

There are different mathematical formulations available to describe the mechanical behaviour of the system. Some of them are based on *energy* and work (virtual work principle, Lagrange's equations) while other are based on partial *derivatives* (Castigliano's method, Railegh-Ritz) [5].

Virtual work principle, suitable to describe static structural problems is based on the assumption that the energy provided on the boundary of a system (mechanical work $\partial L_e = \delta u \cdot Pressure \cdot dA$) is equal to the sum of the energy accumulated on each volume inside the boundary (work $\partial L_i = \delta\varepsilon \cdot \sigma \cdot dV$). Adding the external forces of volume ϕ (such as gravity) and integrating on all the system:

$$\int_A \{\delta u\}^T \{P\} dA = \int_V \{\delta\varepsilon\}^T \{\sigma\} dV - \int_V \{\delta u\}^T \{\phi\} dV \tag{1.3}$$

The second set of equations are representative of the geometry of the elements and describe how they can deform. In FE an element is described by a number of points, called nodes, which are connected together to form a n-dimensional solid. To make some example, a triangular element is comprised of 3 nodes in the cartesian plane connected by 3 edges. A tetrahedron is composed by 4 nodes in the space, connected by 6 edges which forms 4 triangles. To each node is assigned a value (in our case the displacement). The value in a generic point inside the element depends only from the values at the nodal points. Moreover it is a linear function of the nodal values (but may not be linear respect to the probing position) so it can be written as a matrix $[n]$ called *shape function*:

$$\{u\} = [n]\{s\} \tag{1.4}$$

where $\{s\}$ is the vector containing the nodal values and $\{u\}$ is the value calculated for a generic point inside the element. In the elastic problem, the displacement $\{u\}$ is required also to calculate the adimensional strain ε, featured in equation 1.3:

$$\{\varepsilon\} = [\partial]\{u\} = [\partial][n]\{s\} \tag{1.5}$$

The next set of equations that links the strain to the forces (stresses) are the contitutive laws, and are representative of the material. They are expressed by linear functions, which are packed inside a matrix $[E]$ called *elasticity matrix*:

$$\{\sigma\} = [E]\{\varepsilon\} \tag{1.6}$$

The relations presented up to this point are combined together and are ready to be solved. However an exact solution may be impossible to be reached because an

approximation has been introduced: the shape function constrains the displacement of the element, causing a stress error respect to the ideal solution. This residual error can be controlled by choosing the appropriate shape function and by increasing the number of element in the model. Under particular conditions the approximate solution will converge to the exact solution.

Several types of elements have been developed in the years, according to different needs. Often they are based on triangular or square shapes.

1.4.1 Solid Elements

For the analysis of solid models the most commons are the tetrahedron element and the hexahedral element.

Hexahedral elements can have 8 nodes and has the ability to represent linear gradient of stresses inside the volume or it can have 20 nodes (16 placed at the midpoint of the edges) and can provide stresses with a quadratic trend. In fact this two variations are often called *linear element* and *quadratic element*. This element adapts well to solids with perpendicular edges, sweeps or solids obtained through revolution. It is difficult to mesh complex topologies with hexahedral elements.

Tetrahedral elements have 4 nodes or 10 nodes. The 4 node tetrahedron is capable of representing only a constant strain field, and the 10 node tetrahedron a linear stress field. This type of element is very versatile and is the common choice for practical mechanical problems. Automatic meshing is provided by most software dedicated to FEA. However, a greater number of elements is usually required in comparison to hexahedral elements.

When components with thin features have to be analyzed, in the best case scenario the stresses due to bending loads have a linear trend along the section of the thin feature. To accurately represent this gradient at least 3 or 4 constant strain tetrahedral elements are required to have an accurate insight, but more may be required for particular problems. This fact lead to an increase of the total number of elements, which leads to higher computational costs.

For this reasons the simulation of lattices and cellular structures, which have organic shapes and thin walled features is particularly expensive in terms of performance and, when the number of unit-cells reach the hundreds, may become impossible without dedicated hardware.

1.4.2 Shell Elements

To decrease the complexity of the mesh to be analysed with finite elements, it is possible simplify some of its features with alternative elements. For example

beams have only 6 DOF on each node and can approximate a component with constant section loaded and constrained at the ends. To approximate features with one dimension that is small in comparison to the others, *shell elements* can be used. Plates are shell elements with 4 nodes and 6 DOF at each node. A thickness value must be provided and, depending on the element type can be constant or can change at each node. There are two plate formulations historically developed.

The *Kirchhoff formulation* states that for thin elements the shear stresses are negligible in respect to normal stresses. In the deformed configuration this means that the transverse sections always stays perpendicular to the mean surface of the plate. By neglecting part of the stresses, the element is stiffer than the real component.

The *Mindlin formulation* takes into account also the effect of the shear stresses, which are non negligible when the element is moderate-thick. This is used by most FE solvers and is better suited for real cases. To increase precision a quadratic plate with 8 nodes is also available.

1.4.3 Simulation Approaches

While Finite Elements is a useful tool to predict the behavior and the stress distribution of stresses inside a components, it shows some limitations when applied to lattices. The first regards the number of elements because the geometry complexity and the number of details of a real application can require really small elements and huge level of details to be effectively simulated. Some lattices can be approximated with 'exact' elements like beams, which reduce the computational problem at cost of precision, but for Minimal Surfaces geometry that approach is not viable. Moreover the connections between beams often play a crucial role in the mechanical behaviour of the lattice and must be simulated using a more sophisticated approach than just connecting the nodes of the beams [6]. Using 'default' elements tetra/hex to successfully describe a general bending behaviour requires to have 3+ elements through the thickness, and for components comprised of thin walls this requires million of elements if not more.

There are partial solutions to this limitation that involves simulating the single unit cell and extracting general rules to be applied on a simplified models. One of them is called *homogenization* and suits particularly well the analysed lattice topology.

1.5 Additive Manufacturing

There are various additive manufacturing technologies commercially available and capable of printing lattice-structure materials. Two of them are particularly suitable

to manufacture polymeric objects. They are particularly cheap and suitable for small laboratories: Fused Deposition Modelling and StereoLitography Apparatus.

1.5.1 Fused Deposition Modelling

Fused Deposition Modelling is a technology employed for manufacturing parts with thermoplastic materials by depositing a continuous filament of melted material. FDM uses a heating chamber with a nozzle to liquefy polymer that is fed into the system as a filament. The filament is pushed into the chamber by a tractor wheel arrangement and it is this pushing that generates the extrusion pressure.

A large range of thermoplastic materials are commonly printed with this technology: ABS, PLA, TPU, PETG, PA. The feeding filament can even be mixed with fillers, such as carbon fibers, glass fibers and others. The price starts from 10$ /kg and grows for more quality materials.

This typology of machines became progressively cheap and are now spread to the great public. The great strength of the manufactured materials and the scalability in size of the process makes one of the best choiches for many applications.

The main downsides are:

- the processing of the g-code required to run the nozzle movement. This process requires custom software and experience in configuring the right parameters;
- the size of the features must be greater than the nozzle size to be correctly printed. A nozzle with smaller diameter can help but the number of layers required increases, so as the printing time.

1.5.2 Stereolitography Apparatus

StereoLitography Apparatus is an addictive manufacturing technology that relies on Termoset polymers, which sinterize when exposed to high energy electromagnetic beams, which usually falls on the UV range (around 405nm). An evolution based on the same principle and materials of the SLA is MSLA (Masked SLA) which is based on a LCD screen to filter a wide UV lighting source and sinterize only certain areas. The main avantage of this technology is that there is no necessity to calculate a path for the sinterizing ray, but a simple image of the object layer is displayed on the High Resolution LCD screen, which imply:

- sintering of all the layer at the same time, meaning faster printing;
- no need for a routing algorithm and the possibility to export slices images directly from the geometry generation software. Indeed to generate a g-code, commercially available slicers requires a mesh file in input. For big lattice

geometries such mesh can reach several millions of elements, and exporting-importing operations on such geometries can be impossible, and for sure is resource consuming. The nature of implicit bodies instead makes particularly easy to perform a voxelization or to extract one layer at a time, generating a discrete image of the desired resolution. The image does not require to be stored but can be directly sent to the MSLA machine from the modelling software.

- Less moving components meaning less wear and calibration required.

Downsides of this technology are the post-processing operation required for the parts. In fact the liquid materials are volatile and irritants and must be handled with proper cautions. After the component is removed is usually washed with a solvent (isopropyl alcohol) and then exposed to a further curing with mild temperatures and UV lighting. The same precautions must be used for the unused resin before the disposal. A large number of liquid resins are available in the market, ranging from brittle and fragile to vulcanized-like rubbers.

Hobbistic level MSLA Machines became particularly cheap in the last years for the low number of components, and start from few thousands dollars for professional apparatus.

For what concerns the resolution, a detail precision starting from < 50nm is universally achieved and z-resolution can be increased generating some sub-steps. After all this considerations, for the actual application, MSLA technology is considered to be the best fit, however for practical reasons (availability) a FDM is employed.

Chapter 2

Lattice Structures

Lattice structures, also referred as *cellular material* or *lattice metamaterials*, have aroused interest for a long time, with a literature going back to the 80's when Gibson (*MIT*) and Ashby (*University of Cambridge*) started to investigate and describe the microscopic structure of polymeric foams and of natural solids such as bones and woods[7]. Indeed, the word *cellular solids* arose from the structure of natural cells, which are the basic structural elements of many living tissues, such as bones, muscles, woods.

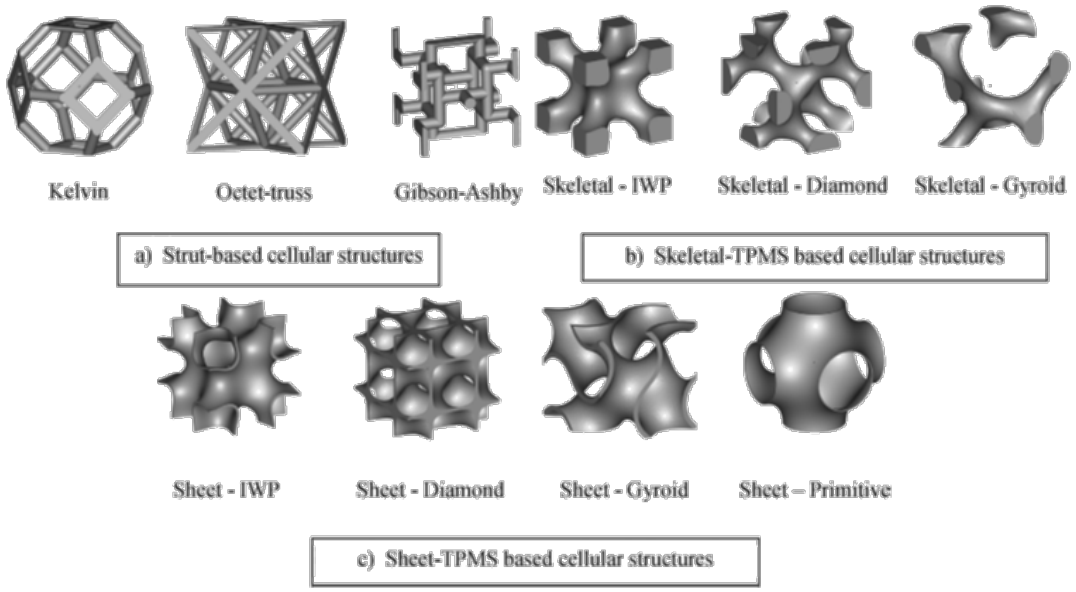

Figure 2.1: Different topologies of unit cells, some based on trusses and others on Triply Periodic Minimal Surfaces. Image from [8]

Gybson and Ashby define a cellular solid as "a solid made up of an interconnected

network of solid struts or plates which form the edges and faces of cells"[1]. This definition will result limited but for now it is useful to outline the following characteristics:

- there are solid structures made of a base material, the residual volume is comprised of gas, or liquid;
- these structures are connected in an organized way, like scaffolds and fill all the solid volume:
- there is a periodic pattern that repeats: the minimum repetitive geometry is called *cell*.

The word metamaterial is also an accurate synonym, since the focus of interest in this field is not the basic material of the specimen, which can be made out almost of anything, but the correlation between the geometry which comprises the solid and it's effect on mechanical properties and functionalities.

Lattices are studied in photonics, a branch of physics about emission, transmission and modulation of photons, because a metal lattice interacts with the electromagnetic field in particular ways and it's possible to bend and filter electromagnetic beams with minimal energy loss. For this applications it's essential to vary the orientation and the period of the lattice in the three-dimensional space with the so called *Spatially Variant Lattices*[9].

The interest in the mechanical field is linked to Additive Manufacturing, which is the preferred manufacturing process since no other process can make these macroscopic complex geometries with many undercuts.

The description and investigation of properties is conducted at a macroscopic level with the help of some macroscopic features. The most important is the *relative density* denoted as $\rho_r = \rho^*/\rho_s$ that is the ratio between the density of the cellular solid and the density of the constituent material. Common values can range from 10^{-2} for packaging and insulation to 0.4 for woods, but usually the range of study is $\rho_r < 0.3$. The description of the structure can focus on the geometry of the *unit cell* and how the material is distributed or can investigate the intrinsic properties at a macroscopic level. We will proceed in listing this macroscopic features, which later will be adopted to study the behaviour of the material and used to develop the relations that correlate one to the other.

- Density of the metamaterial ρ_s or relative density of the metamaterial calculated as the ratio between the density of the lattice sample and the density of the constituent material.
- Young's Modulus E_s
- Plastic strength

- Fracture Strength

According to research done by Gibson& Ashby the mechanical properties (Young's Modulus, strength, toughness) can be approximated by relations in the form:

$$\Phi_{lattice} = \Phi_{solid} C \rho_r^n = \Phi_{solid} \cdot C \left(\frac{\rho^*}{\rho_s} \right)^n$$

where Φ_{solid} refers to the property of the solid constituent material and C, n parameters depend on the material and on the lattice geometry.

Degrees of Freedom. When generating lattices it is convenient to list the parameters that can be independently tuned.

- The first is the *unit cell*, which can also be described by the *unit cell field*.
- The second parameter is the *relative density*, which is directly linked to the *threshold value* at which the field is divided between inside and outside, thus generating the binary lattice.
- The third and fourth parameters are the *cell size* and the *orientation angle*. This two variables are strictly connected because they can be seen as a **grading vector** on the space with magnitude and direction corresponding to cell size and orientation angle.

2.1 Triply Periodic Minimal Surfaces

A well-known and studied class of cellular structures is based on *Triply Periodic Minimal Surfaces*. These Surfaces are defined by analytical equalities in the 3-dimensional Cartesian plane

$$f(x, y, z) = T$$

where f is a periodic function and T is a scalar value, often equal to zero. However the function $f(x, y, z)$ is defined for all the points in space and defines a scalar field. Moreover the solution domain of f is such that the divergence is always null . On a geometrical point of view this means that the surface has no local minimum point. Some notable TPMS equations are the

- Schoen-Gyroid:

$$\sin X \cos Y + \sin Y \cos Z + \sin Z \cos X \tag{2.1}$$

- Schwarz-Diamond:

$$\cos X \cos Y \cos Z - \sin X \sin Y \sin Z \tag{2.2}$$

On these two geometries many studies have been conducted, mainly with an heuristic approach, with experimental tests and Finite-Element simulations, because there is a lack of a unified mathematical model for predicting the behaviour of a general Lattice geometry.

Since the values of the scalar field are always [-1,1] but the period of the field is scaled in size, from geometrical considerations:

$$\chi = threshold\ value = C_1 \cdot \frac{thickness}{cell\ size} = C_1 \frac{t}{l} \tag{2.3}$$

with a parameter $C_1 \approx 3$ for a Sheet Gyroid geometry. In this way it is possible to obtain relative densities that are as small as desired, always keeping in mind that the cell size increases as $1/x$ for a diminishing relative density. It is therefore necessary to check that the cell size remains smaller than the volume geometry in order to keep the mechanical behaviour predictable.

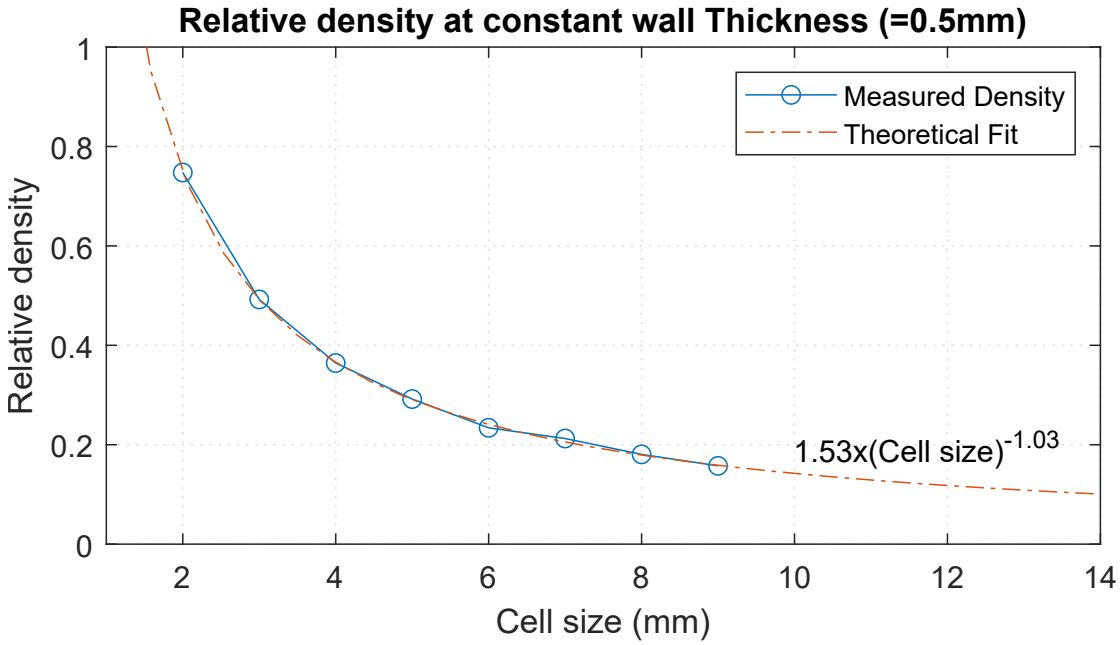

Figure 2.2: Cell edge size vs. density

To calculate the relative density of the lattice from the previous parameters a further relation is needed. In fact, this relation depends on the structure topology (*honeycomb*, *open cells*, *closed cells*), that in our case have to be defined. Generating

various constant-thickness lattices (0.5 mm) in *nTopology* and performing a volume integral, the following data have been extracted (figure 2.2).

An interpolation with a base function $a \cdot x^b$ revealed a trend like $1/x$ (a=1.526, b=-1.03). According to Gibson this relation is compatible to *Closed-Cells* structures, and leads to the following formula[1]:

$$\rho_r = C_2 \frac{t}{l} \tag{2.4}$$

where in this case $C_2 = 3.05$. The interesting fact to notice is that $\chi \approx \rho_r$ because $C_1 \approx C_2$.

2.1.1 Design of TPMS

Designing a simple Triply Periodic Minimal Surface is quite easy. The analytical equations provided before are the fundamental of the workflow. As seen in figure

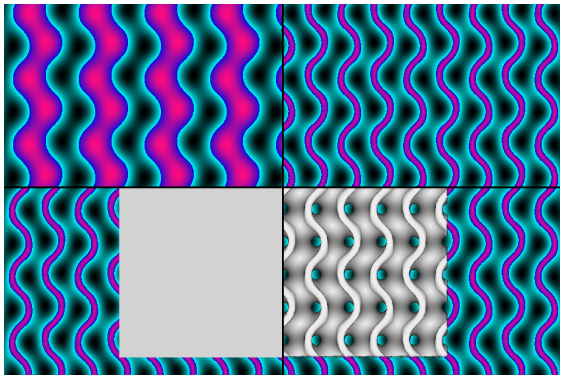

Figure 2.3: From left to right, from top to bottom. The stages of generating a lattice solid.

2.3 the analytical expressions generate a 3d *Scalar Field* which is a function $f = f(x, y, z)$ with one scalar output value (a). For the gyroid, the values of this field are in the interval [−1,1] and the null values form a surface which divide the space in two separated contiguous domains. To obtain a thin-sheet solid it's necessary to take all the points close to this surface. Remember that for definition an implicit body has negative value inside the boundary surface and positive values outside. To make negative all the points within a specified threshold value t^* it's possible to subtract it from the absolute value of the gyroid field.

$$g_{sheet} = abs\left(g(x, y, z)\right) - t^* \tag{2.5}$$

The function g is the scalar field of gyroid in equation 2.1 and g_{sheet} is the scalar field of the thin walled gyroid (b). This field can be intersected with another implicit body

to create a boundary for the gyroid field (c) (d). Performing boolean operation on implicit bodies is particularly easy and robust operation. The intersection between body A and B in this case is defined as:

$$A \cap B = min(abs(A), abs(B)) \ \cdot \ max(sign(A), sign(B)) \tag{2.6}$$

The new implicit body will have negative signs only if both fields are negative and value equal to the minimum value of the values. To generate a binary solid, all the negative values are considered as inside (solid) and the positive values are considered outside. This step is strictly connected to the generation of a mesh or a discretization, and it's maybe the most memory intensive operation, since the mathematical formulation has to be computed for each point. One way to create a mesh to export is to evaluate the field at each point of a 3-dimensional matrix. Each point of this matrix is callex *voxel*. When the field has been estimated inside the region of interest, it's possible to connect all the vertex that lies at a certain value (for implicit bodies this value is 0) and connect them to generate a surface mesh. The mesh structure, composed of vertex and triangles/quadrangles is ready to be exported as .stl or .obj file format. The functions to generate the mesh from the voxelization in Matlab are `isosurfaces()` and `isocaps()`. Also nTopology provides embedded functions to voxelize and mesh the implicit solids.

This is the easiest way to obtain a lattice with constant cell size and constant thickness. With few modifications it's possible to spatially vary this parameters.

2.2 Spatially Graded lattices

Spatially grading consists in changing the size, shape, direction and density of the lattice in order to obtain particular properties. There are many reasons to grade a lattice:

- reducing the weight while maintaining a target resistance, often by varying the thickness according to results of simulation or *Topology Optimizations*;
- tuning the stiffness and the energy absorption characteristics, in cushioning and impact-absorbing applications;
- deforming the orientation of the principal axis to support stresses which has a specified direction[10] or adapts to a particular shape (conformal lattices)
- obtaining other non-mechanical phenomena, for examples when metal lattices interact with an electromagnetic field, in the research area of photonic crystals [9] ;
- controlling the interaction with other substances in applications where multiple fluids are involved, as in heat exchangers.

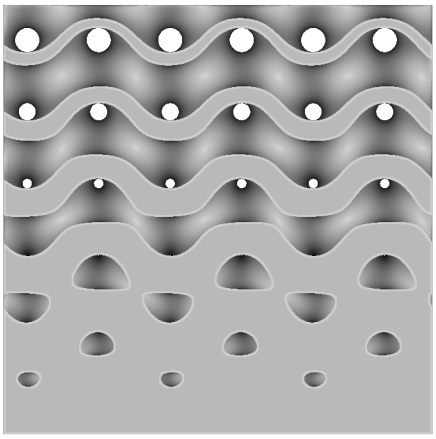

Figure 2.4: Grading thickness of a gyroid lattice in the z direction.$t^* = k \cdot z + t_0$

Let's start discussing about tuning the thickness of the lattice or equivalently the relative density. This process is quite easy and is done by locally varying the threshold value $t^* = t^*(x, y, z)$ in equation 2.5. t^* generates an offset of the lattice field, to expand or retract the boundary between negative and positive values. Since there is a minus in the field equation, an increasing t^* increases the lattice thickness.

To change the orientation and shape of the lattice a different approach is required. As defined, a lattice is the sum of a basic cell, repeated in space. The boundary of this unit cell is a square in 2D and a cubic box in 3D, which is repeated along the directions X,Y and Z with period p. One approach is to have some elements, like trusses and beams defined by nodal coordinates in the unit cell, which must be duplicated for every periodic cell boundary. For a regular repetition the nodal coordinates are the combination of the periodic position indexes

$$combinations([X_0 + p \cdot n], [Y_0 + p \cdot n], [Z_0 + p \cdot n])$$

where p is the period and n is a list of integers containing the indexes to the unit cells. This approach is time consuming and suffer severe limitations when trying to modify and grade the period, specially when nodal coordinates are generic points within unit cell boundary box.

The advantage of using a periodic function with an analytic description, such as TPMS, is that it's particularly easy to evaluate the value of the function for every point is space and to modify the lattice shape. To understand how to modify the shape of a lattice we will refer to a one-dimensional case which is easier to understand, but the generalization for greater dimension will be intuitive. Let's start by noticing that gyroid equation is comprised of sinusoidal functions with a

singular argument (for example $\sin(\phi)$). Let's call the argument of the function, *phase*. The periodicity of the sinusoidal function happens when the value of the phase changes by a value of 2π. When the phase is a linear function such as $\phi = a \cdot x$ then the periodicity happens when $2\pi = \Delta\phi = \Delta(a \cdot x) = a\Delta x$ so that $\Delta x = 2\pi/a$. In fact, when the coefficient a increases, there is an inverse reduction of the period of the sinusoidal function (a is proportional to the frequency).

It is possible to generalize this concept to any function ϕ: the periodicity happens when the value of the function changes by 2π. Converting this statement to formula and expressing ϕ as a generic function of x as $\phi(x)$:

$$2\pi = \Delta\phi = \int_{x_0}^{x_1} \frac{\partial\phi(x)}{\partial x} dx = \int_{x_0}^{x_1} K(x)dx \tag{2.7}$$

The derivative of ϕ is called $K = K(x)$. This value represent how fast the phase is changing in respect to x and thus is proportional to the instantaneous frequency, and indirectly to the length of a full period. Going from the end to the beginning: it's possible to impose an arbitrary law $K(x)$ to control the local frequency of $\sin(\phi)$ function. It's just required to define the value of the phase integrating $\phi(x) = \int K(x)dx$. It's possible to visualize the deformed period as checked lines (black, white).

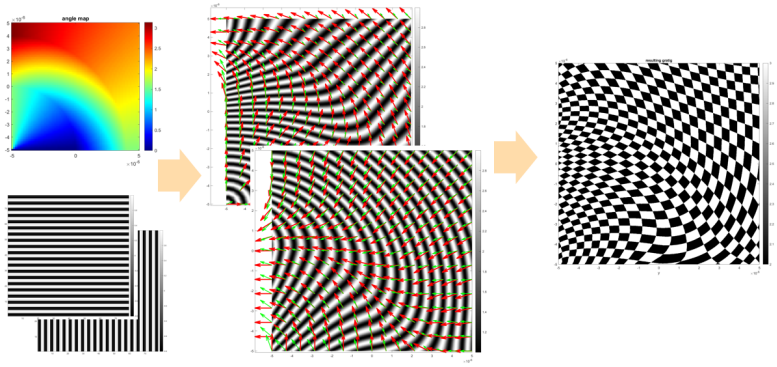

Figure 2.5: In this 2d example, the planar XY grating is varied with an orientation map to obtain a new spatially varied grid. The principal grating vector $\vec{K}$ has unitary length and direction controlled by a 2d angular map (first graph). The grating vectors $\vec{K_x}$ and $\vec{K_y}$ are integrated separately and then recombined in the final grating.

Let's try to expand the concept to a 2-dimensional case, where there are two axis x and y which, when superposed, form a *grating plane* (just like a checker board). These two grating directions are represented by the arguments ϕ_x and ϕ_y. Each of them is a 2-d scalar function such as $\phi = \phi(x, y)$. Replicating the same

reasoning done before we define:

$$\vec{K_x} = \left(\frac{\partial \phi_x(x,y)}{\partial x}, \frac{\partial \phi_x(x,y)}{\partial y} \right) \tag{2.8}$$

and call it *grating vector*. Similarly we define a second grating vector $\vec{K_y}$ that, in expressed in polar coordinates, represents the frequency and orientation of the grating along the direction y. Usually $\vec{K}$ is defined by design and ϕ is calculated by performing an approximate integration on the xy plane by using numerical methods such as *finite differences*. The downside is that the solution is not an analytical formula but is a discrete matrix of values, but local interpolation to increase resolution is possible.

With this approach we obtain two grating vectors $\vec{K_x}$ and $\vec{K_y}$ that are independent from each other (generally not orthogonal) and may cause a skewed and inconsistent grating. To avoid this, it is preferred that $\vec{K_x}$ is perpendicular to $\vec{K_y}$, just like x is perpendicular to y. By adding this condition the unit cells tend to maintain their original orthogonality. The equation:

$$\vec{K} \rightarrow \begin{cases} \vec{K_x} = i \cdot \vec{K} + j \cdot \vec{K} \\ \vec{K_y} = j \cdot \vec{K} - i \cdot \vec{K} \end{cases} \tag{2.9}$$

shows that it's possible to define a principal grating vector, which is sufficient to define the deformation of the grating. This process has been implemented in Matlab for a 2d case and shown in figure 2.5. The expansion in the third dimension is relatively easy to perform.

On the basis of what has been seen, the full expression of a spatially varied gyroid implicit lattice is:

$$\begin{aligned} G'(x,y,z) = \sin(\phi_x(x,y,z))\cos(\phi_y(x,y,z)) + \sin(\phi_y(x,y,z))\cos(\phi_z(x,y,z)) + \\ + \sin(\phi_z(x,y,z))\cos(\phi_x(x,y,z)) - t^*(x,y,z) \end{aligned}$$

which is particularly powerful because defines with a single expression all the lattice field inside the boundary region.

2.3 Mechanical Behaviour

One may look at these complex geometric shapes and tridimensional patterns and wonder how this geometry behaves under a mechanical load. Only recently such geometries have been manufactured extensively and the number of experimental research on the topic is increasing. The stresses running through the walls are hardly predictable without an accurate modelling and study through simulation

(FEA) and even in such case it's difficult to predict precisely the collapse behaviour and the failure points, because this characteristics are heavily influenced by the geometric imperfections and by the manufacturing process.

However, a general model for predicting the behaviour of foams and cellular solids has been provided by different authors and unified by Gibson and Ashby [1] more than two decades ago. In that case, the focus was on *foams* and natural cellular solids, but in reality the theory underlying is perfectly compatible with the experimental data that we obtained

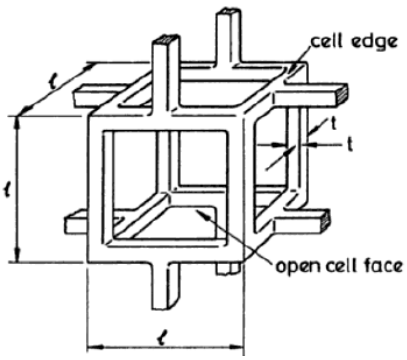

Figure 2.6: The model of foam invented by Gibson [1] to extract the theoretical equations for the stiffness and strength of foams.

The main characteristic when making a model of the mechanical properties is the topology of the foam: *open-cell* or *closed-cell*. In fact, closed-cell foams may contain fluid trapped inside the cells that when compressed, respond with a pressure according to the ideal-gas or incompressible fluid law. Moreover the walls are part of the structure and contribute to the general stiffness. Open-cell foams are modeled as an assembly of structural beams, as shown in figure 2.6. From basic structural evaluations it's possible to extract theoretical formulations for Young's Modulus, Plateau Stress and Densification.

The base to describe mechanical properties is to draw some basic geometrical relations from beam theory. The relative density is proportional to the volume of the beam elements and the *Area Moment of Inertia* I, which impacts the stiffness, is proportional to the edge size to the fourth power:

$$\rho_r \propto \left(\frac{t}{l}\right)^2 \tag{2.10}$$

$$I \propto t^4 \tag{2.11}$$

Under a compressing load, the vertical beams (referring to the Gibson Model of image 2.6) transmits the forces to the midpoint of edges of the cell. The

displacement is caused by this edge of the cell bending under a load F. The case is equivalent to a bi-dimensional beam with fixed ends and loaded in the center. Since the beam is symmetric and can be cut in half, it's equivalent to a cantilever beam (of length equal to the half of the edge) with rotation inhibited at the free end. Recalling the basic formulation of the beam theory (Euler-Bernoulli), the stiffness matrix is

$$EI_z \begin{bmatrix} \frac{12}{L^3} & \frac{6}{L^2} & -\frac{12}{L^3} & \frac{6}{L^2} \\ \frac{6}{L^2} & \frac{4}{L} & -\frac{6}{L^2} & \frac{2}{L} \\ -\frac{12}{L^3} & -\frac{6}{L^2} & \frac{12}{L^3} & \frac{4}{L} \\ \frac{6}{L^2} & \frac{2}{L} & -\frac{6}{L^2} & \frac{4}{L} \end{bmatrix} \begin{Bmatrix} \delta_1 \\ \alpha_{z1} \\ \delta_2 \\ \alpha_{z2} \end{Bmatrix} = \begin{Bmatrix} f_{\delta 1} \\ m_{z1} \\ f_{\delta 2} \\ m_{z2} \end{Bmatrix} \tag{2.12}$$

where f_δ and m_z are the vertical force and the moment around the normal axis on the beam ends 1 and 2, δ and α_z are the corresponding vertical displacement and rotation of the nodes 1 and 2. The value E is the Young's Modulus of the constitutive material, I_z the Area Inertia of the section of the beam, and L is the total length.

In the case described before, with one node (1) completely constrained and the other (2, corresponding to the cell edge mid-section) with inhibited rotation, results that $\delta_1, \alpha_{z1}, \alpha_{z2} = 0$ so only one degree of freedom is left, which corresponds to the third column of the stiffness matrix. The relation between force and displacement is therefore:

$$\delta = \frac{1}{12} \frac{L^3}{EI} f_\delta \tag{2.13}$$

Moreover $L = \frac{1}{2}l$; $f_\delta = \frac{1}{2}F$; $\varepsilon = \delta/l$ where ε is the adimensional strain of the unit cell. Combining this relations together we obtain that

$$E^* = \frac{\sigma}{\varepsilon} \propto \frac{E_s I}{l^4}$$

and adding relations 2.10 and 2.11 it follows that

$$\frac{E^*}{E_s} = C_1 \left(\frac{\rho^*}{\rho_s} \right)^2 \tag{2.14}$$

where value C_1 is a generic constant of proportionality.

It is important to note that during the calculation of this result the only contribution on the deformation is due to the bending of the horizontal edges and the axial compression of the vertical beams has been neglected. This approximation is valid because for axial compression $\delta_N = \frac{l}{EA} f_\delta$ which for slender beams is negligible in respect to δ, at least for elastic small displacements. In fact for higher loads, buckling tends to occur to vertical beams and local collapse happens. This relation does not hold true for lattices which are stretching dominated, meaning

that no bending phenomena occurs (an example is the *Schwartz* skeletal lattice, which can be imagined like the union of axial trusses aligned along the principal directions X,Y,Z).

Another approximation is performed on the vertex of the cell, where masses of the beams are counted multiple times. The third important hypothesis that has been made is that the material can be treated as a continuum, but this holds true only where the cell size is small relative to the size of the specimen. Studies have shown that the ratio between specimen diameter and cell size must be more than 20 to obtain accurate results. In fact, in the boundary of the lattice an uneven distribution of stresses is aroused, possibly creating an *edge effect*. This assumption is also used in other numerical approaches to study lattices, such as the homogenization method.

This model is more useful to underline the basic relations to be tailored on the experimental results, more than providing accurate numerical results. However an extremely good fit will be shown in the following chapter.

The equivalent shear modulus can be calculated in a similar way, and for open cells is

$$\frac{G*}{E_s} = C_2 \left(\frac{\rho^*}{\rho_s}\right)^2 \tag{2.15}$$

from which is possible to calculate an equivalent Poisson's ratio ν^* from the relation $G = \frac{E}{2(1+\nu)}$. Gibson et Ashby discuss also some ways to manufacture foams with negative Poisson's ratio, which are called *Auxetic*.

Moving from linear elastic response with increasing loads, there is a flattening of the stress strain occurs which culminate on a peak, when elastic or plastic buckling occurs. This condition is described by the buckling theory with the relation between load F and beam characteristics:

$$F_{crit} = \frac{n^2 \pi^2 E_s I}{l^2} \tag{2.16}$$

where n^2 is a value representative of the boundary conditions at the beams ends. Anyway, since stress is calculated as Force/Area it holds that

$$\sigma_e l^* \propto F_{crit}/l^2 \propto \frac{E_s I}{l^4}$$

which combined with relations seen before results in

$$\frac{\sigma^*_{el}}{E_s} = C_4 \left(\frac{\rho^*}{\rho_s}\right)^2 \tag{2.17}$$

where C_4 express the proportionality factor. When a single failure happens, the entire lattice layer undergoes an increase in stresses and tends to collapse as well.

From experimental evidence this phenomena occurs in planes perpendicular to the load direction or in shear-bands that runs across multiple layers. This characteristic is said to be independent of the relative density and dependent on the cell topology [8]. Also, the collapse mechanism may depend on the constitutive material of the lattice, as there are discrepancies between our research and investigations performed on different materials.

The subsequent collapse of multiple layers creates a region where stresses are constants, at least for *open-cell* foams, until a full densification occurs. This unique characteristic allows to absorb a lot of energy at a constant stress level and is exploited for crash protection and energy-absorption systems.

Another type of collapse can occur for materials with low strain values and is *plastic collapse*. It happens on the structures affected by bending, when the yielding stress is reached, at the full-constrained node of the beams. Other times, when the material is extremely brittle, a sudden rupture occurs in the same areas.

Further studies can be found in specialized books [1] [7] and specific papers. The aim of this section was to show how it was possible to approach a complex system with a simple model using basic principles of mechanics and well-known relations. In particular was focused on open-cell foams (and from the mechanical viewpoint a Gyroid lattice behaves like an open-cell foam) and materials which undergoes big elastic strains and elastic buckling. For a lot of applications this model will provide an accurate description, as seen in the following chapters.

2.4 Numerical Simulation

The previous section explained how it was possible to create an analytic model of a lattice and how to extract some reference curves which predicts the behaviour of a generic lattice. The discussion was particularly focused on open cell foams because they are topologically more similar to a gyroid.

A different approach to predict the behaviour of solid lattices is based on simulation. Various simulation models are possible; some of them relies on statistical methods, semi-analytical or fully numerical methods.

Finite Element Method is a powerful tool to compute the mechanical response of many different physical systems. In fact the component is subdivided in many simple solid elements that approximates the local behaviour of the system. However, as the complexity of the geometry increases, the computational effort grows and becomes difficult to sustain. This particularly holds true for lattices where the number of elements scales up with n^3 The problem is less relevant when the model is idealized and approximated by beams and shell elements (instead of solid) because the reduction of the number of elements and the d.o.f. (degrees of freedom) improves the performance. However this simplification may lead to incorrect

results, especially when non-linear behaviour is investigated. Some models uses an hybridization of thin elements and solid elements in the critical areas. One aspect of this kind of modelling (of the full component) is that the boundary conditions and the geometrical variations of a graded lattice, which may be important in the mechanical behaviour, are accurately modelled.

A different approach is more concerned in treating the material as an infinite medium. The study of the microscopic behaviour of the unit cell leads to define the behaviour at the macroscopic level. Geometrical periodicity and periodicity in boundary conditions ensure that the microscopic properties can be extended to all the volume filled by the lattice (theoretically infinite). This process is called *homogenization*.

2.4.1 Homogenization

The effective physical behaviour of lattice structures on the macroscopic level can be treated as a homogenized pseudo-material, with an equivalent Young's Modulus and Shear Modulus along the principal directions. This equivalent material is also used in FE simulations treating the lattice as a solid region, thus reducing greatly the number of elements.

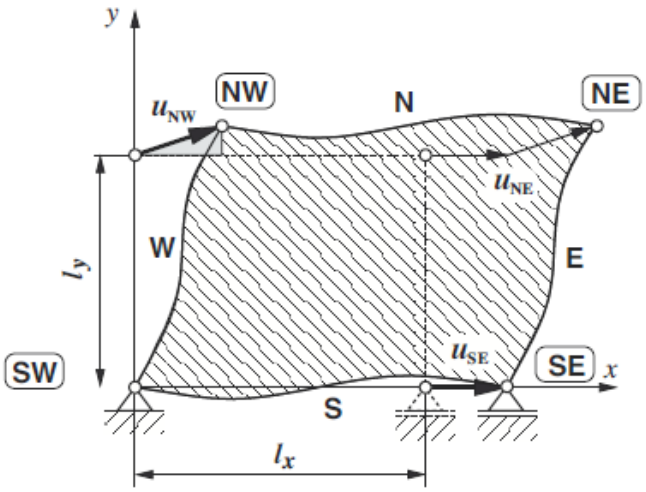

Figure 2.7: Idealized representation of a 2d unit cell in undeformed and deformed configuration. Boundary conditions are applied between opposite edges. Image from [11]

The core idea behind homogenization is to take a periodic unit representative of the repetitive structure and, by applying some periodicity boundary conditions. In a bidimensional model (represented in figure 2.7) unit cell is contained in a rectangular area with four nodal vertex and four edges. The mesh node coinciding with vertex

SW is fixed in order to prevent rigid body motion. Vertex SE is constrained along y direction and the other two vertexes have a prescribed displacement. It is possible to calculate the strain on the unit cell as

$$\varepsilon_{xx} = \frac{u_{SE}}{l_x}, \qquad \varepsilon_{yy} = \frac{u_{NW}}{l_y}, \qquad \gamma_{xy} = \frac{u_{NW}}{l_y},$$

The nodes that lies at the edges N and E are connected with the nodes at the opposite edges S and W and the values of displacement coincides except for a constant. Edges S,W are master DOF and N,E are slaves nodes:

$$u_E(y) = u_W(y) + u_S E$$

$$u_N(x) = u_S(x) + u_N W$$

Since the displacement of all nodes on the slave edges are coupled to master nodes, the forces acting on the master nodes are distributed over the entire edges and the stresses are summed up until static equilibrium is reached. The unit cell model reacts to concentrated loads in the same way an infinite periodic structure would behave. The resultant forces calculate through Finite Element Analysis are divided by the edge length to obtain the mean stresses

$$\sigma_{xx} = \frac{H_{SE}}{l_y}, \qquad \sigma_{yy} = \frac{V_{NM}}{l_x}, \qquad \sigma_{xy} = \frac{H_{NW}}{l_x}$$

From strains and stresses is possible to calculate the elasticity matrix $[E]$ which contains the characteristics of the homogenized material.

$$\begin{bmatrix} \varepsilon_{xx} \\ \varepsilon_{yy} \\ \gamma_{xy} \end{bmatrix} = \begin{bmatrix} \frac{1}{E_{xx}} & -\frac{\nu_{yx}}{E-y} & 0 \\ -\frac{\nu_{yx}}{E_{xx}} & \frac{1}{E_{yy}} & 0 \\ 0 & 0 & \frac{1}{2G_{xy}} \end{bmatrix} \begin{bmatrix} \sigma_{xx} \\ \sigma_{yy} \\ \sigma_{xy} \end{bmatrix} \tag{2.18}$$

It can be used inside other simulations as representative of the characteristics of the lattice. More often, Homogenization is a useful tool to investigate how a change in unit cell geometry affects the mechanical characteristics. It is not able to predict local defects and crushing behaviour since these are local phenomena, not global.

Expansion to the third dimension is similar to what explained in the 2d case, with the exception that the matrix $[E]$ is 6x6 in size.

Chapter 3

Experimental Work

The following chapter is the core of this paper and investigates the **mechanical properties** of sheet TPMS lattice under uniaxial compression at various densities and testing conditions. Practical topics such as design of specimens, manufacturing, testing and extrapolation of results are discussed. The findings of this chapter will then be used during design of more complex and functional components.

3.1 Design of Samples

As seen in chapter 2, two approaches can be adopted for varying the relative density. The first approach is to fix the unit cell-size and, by varying the threshold cut value, change the thickness of the walls. Choosing a constant cell size is a great advantage in the design stage, but the main drawback is that the thickness of the walls can become particularly thin and hard to manufacture. For example if the edge length is fixed at 5 mm and the desired relative density is 0,1, the wall thickness has to be 0,17 mm, which in our case is below the manufacturing limit.

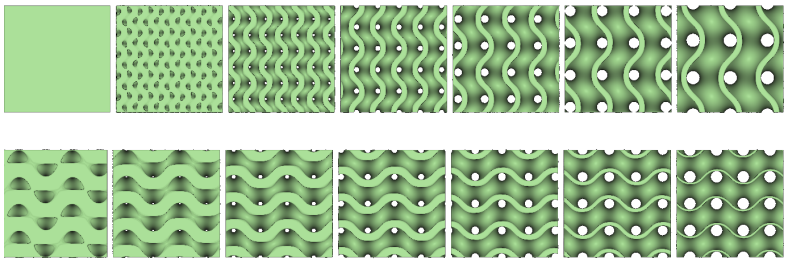

Figure 3.1: Two approaches of controlling the density: a) Fixing the thickness and varying the cell size; b) Fixing the cell size and varying the thickness.

The other approach is to keep a fixed thickness of the walls and to vary the cell

size. This approach is more suitable for FDM printing since it is possible to select a threshold thickness ($1 \div 2$ times the diameter of the nozzle) that displays a good manufacturing result and then spatially vary the lattice cells to obtain the desired relative density.

Anyway, to keep the number of unknowns under control, the cell-size was fixed to (7 mm)x(7 mm)x(7 mm) and the number of cells inside the volume to 5x5x5. Only when the thickness was not suitable to print, the cell-size was modified but the number of cells was kept to 5x5x5, in order to keep the edge effects under control.

The geometry is generated with the software *nTopology*, that provides at least a couple of different tools to generate various lattices. The approach used relied only on basic field operations: a tridimensional gyroid scalar field is generated and, after some manipulations, it is intersected with the boundary box. This process creates a binary implicit solid (a more detailed description of the process is in chapter 2). The volume of this solid is calculated by performing a volume integral and divided by the volume of the boundary box. This value is equal to the *relative density* $\rho_r = V*/V_s$. The binary solid is meshed and exported as .obj together with the data about he size and the theoretical density.

3.2 Manufacturing

The material used to manufacture the samples is a Thermoplastic PolyUrethane(TPU) in $1.75 \pm 0.02mm$ filament from 3dwarhorse, the brand of a Chinese manufacturer[12]. According to the manufacturer, the hardness of the material is 95A in Shore durometer scale. Other information are not provided. The cost is around 48€/kg.

To measure the density a strip of filament is cut and weighted on a laboratory balance.

Diameter	Length	Weight	Density
1.75 ± 0.02 mm	2000 ± 5 mm	6.164 g	1281 $kg/m^3 \pm 2.5\%$

The printer used is a Creality Ender 3, an entry-level machine available as a pre-assembled kit at around 200€. The printing volume is 220x220x250mm, which will prove enough for our application. The main limitation is the extruder step motor, which is placed 15cm away from the nozzle and it has a limited power and retraction efficacy. Nonetheless, the printer performed well after proper setup.

Slicing was performed with the software Ultimaker *Cura 4.8.0*. By default, details that falls below 2 times the Nozzle Diameter are cut out, so the setting *"compensate walls overlaps"* was activated with a *"minimum extrusion flow"* set to 0%. In this way it was possible to print up to 0.3 mm details.

Bridges and suspended areas of the gyroid must be thick enough to be sliced in 3/4 layers in order to guarantee a minimum geometric accuracy. For this reason the layer height was set to 0.12mm.

After several trials, the best printing parameters were : -bed temperature: off; -retraction: off; -nozzle temperature: 210°C; -printing speed: 20mm/s with a nozzle diameter equal to 0.3mm.

Over the span of a couple of days, a various number of cubic and non cubic specimens have been printed. To keep the edge effect under control, the samples are made of at least 5x5x5 unit cells or above. In general a constant-cell-size approach has been adopted, except where the walls were to thin to print and the cell size has been increased. Table 3.1 shows the list of specimens.

ID	Cell size	Threshold	Thickness	# cells	Height	Width	Length	Measured Weight	Theoretical Density	Measured Density	Density Error
	mm		mm		mm	mm	mm	g	%	%	
C011	11	-	0.6	5	55	55	55	24.72	0.158	**0.116**	-27%
D020	4	-	0.5	8.75	35	35	35	7.74	0.183	**0.141**	-23%
A020	7	0.2	0.46	5	35	35	35	7.90	0.193	**0.144**	-26%
C031	7	-	0.6	5	35	35	35	10.27	0.249	**0.187**	-25%
A030	7	0.3	0.7	5	35	35	35	12.06	0.290	**0.220**	-24%
D010	5	-	0.5	7	35	35	35	12.33	0.350	**0.224**	-36%
A040	7	0.4	0.93	5	35	35	35	15.89	0.389	**0.289**	-26%
A040-X	7	0.4	0.93	5	35	35	35	15.89	0.389	**0.289**	-26%
A040-Y	7	0.4	0.93	5	35	35	35	15.89	0.389	**0.289**	-26%
B018	5	0.6	1	5	25	25	25	6.01	0.590	**0.300**	-49%
A040-S	7	0.4	0.93	6	34.6	11.7	34.8	5.57	0.389	**0.308**	-21%
RAMP	-	-	-	-	30	10	10	1.45	-	**0.377**	-
B019	5	0.8	1.33	5	18.3	25	25	6.01	0.802	**0.410**	-49%
CUBE	-	-	-	-	19.8	12.8	19.8	5.67	1	**0.879**	-12%

Table 3.1: All the specimens with related size-mass values.

The last operation was to weight all the printed parts and measure their size with a caliper. The actual weight of the specimen was around 24% lower than the expected value. This has been re-conducted to a systematic under-extrusion of the printer. Also, specimen called *"CUBE"* (on the right in figure 3.2) which was a prism printed with 100% infill and was supposed to have a relative density of 1, showed a relative density of 0.879, a value not explainable with errors. This is probably due to small air gaps between the fused filaments.

3.3 Testing

The machine used for performing compression tests was a *Zwick/Roell Z005* Universal Testing Machine with Maximum test load of 5kN. The tools used were two

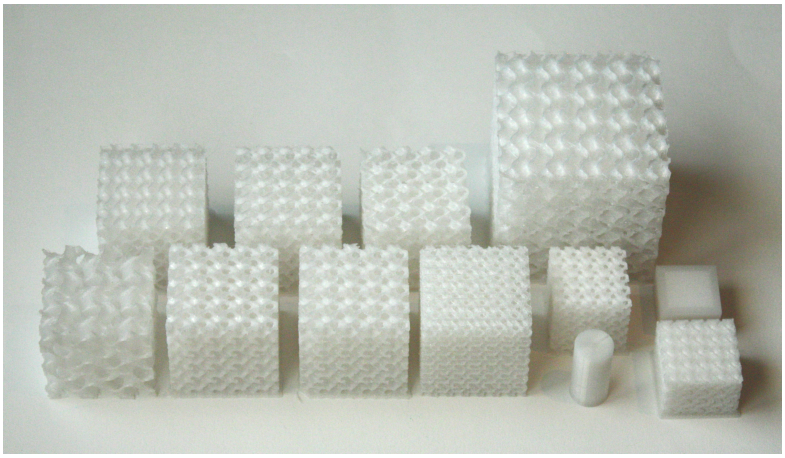

Figure 3.2: View of the specimens prepared to be tested.

parallel and coaxial cylinders of steel which clamped the specimen placed beneath. A camera was connected to record videos and images.

Low Strain-Rate Testing has been conducted at 5mm/min up to densification point where all layers collapsed and the stress started to increase fast (a further compression would have provided more data but may have resulted in permanent damage of the samples). Figure 3.3 presents the main phases of compression. The test started to record data when an approaching load of 1N ($\approx 800Pa$) was reached.

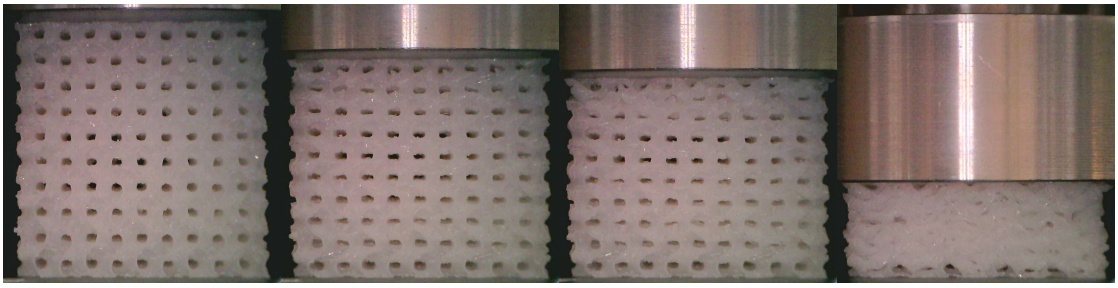

Figure 3.3: Crushing behaviour of specimen A020: a) initial contact; b) linear elastic compression; c) asynchronous collapse of lattice layers; d) full collapse and densification.

Low and High Strain-Rate Cyclic tests have been also conducted to study the energy return of the material and to simulate a possible working condition.

Since the sample did not show measurable permanent deformation in size few minutes after testing, it was possible to study the anisotropy behaviour of the specimens performing tests along the X, Y, Z axis.

Results were stored as separate .csv files and recording as .avi format.

3.4 Results

3.4.1 Static Behaviour

Experimental data is imported in *Matlab* to perform visualization and analysis. Stress and relative strain are calculated based on nominal size of the specimen. A selection of 7 specimens manufactured with the same parameters and with cell size of 7 mm have been chosen for further analysis.

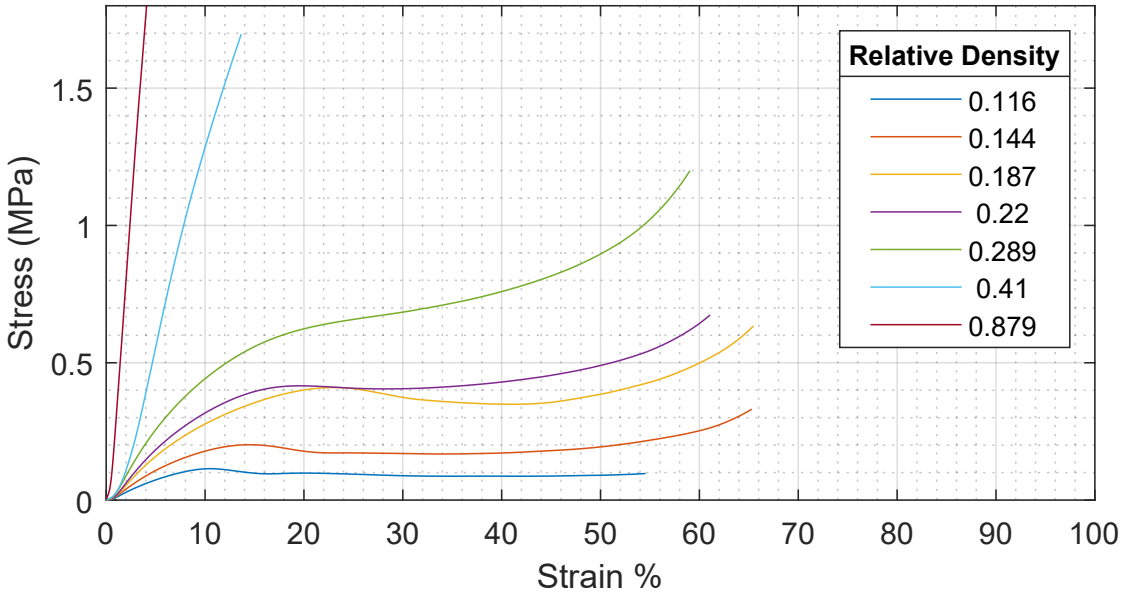

Figure 3.4: Stress/Strain plot for cubic samples of dimension 5x5x5 unit cells.

Figure 3.4 shows the Stress-Strain curves of the specimens, when compressed at the slow rate of 5mm/min. Curves show an initial linear elastic trend, which slowly bends up to the point where one of the layers collapse, as shown in figure 3.3. The collapse, due to buckling of the structure, takes place in horizontal bands. The material is important in the crushing behaviour of the lattice, since findings from other papers[8] obtained collapse along shear-bands in samples made from steel.

The layers proceed to collapse one after the other, causing a plateau in the stress response. When all the layers already collapsed, the surfaces of the sheet-gyroid make contact with each other and, after a transient, the specimen starts to behave as a bulk solid made of TPU with a high Stress/Strain ratio until permanent damage. This last phase is called densification.

Unluckily, the compression tests were interrupted at around 50% strain and thus the data plot about densification phase is missing. However our application does not contemplate such high-pressure conditions and this limit allowed us to discover that no permanent deformation occurred after the removal of the load.

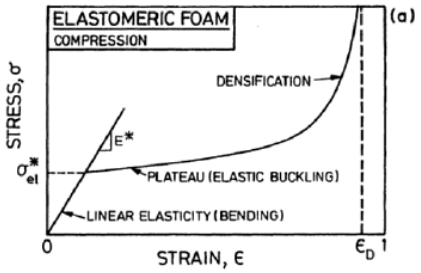

Figure 3.5: Behaviour is compatible with what described in Gibson & Ashby [1].

3.4.2 Young's Modulus

The Young's modulus, calculated on the strain interval $[1.5, 3]$ is plotted as function of the relative density. As seen in chapter 2, Gibson and Ashby found out that the

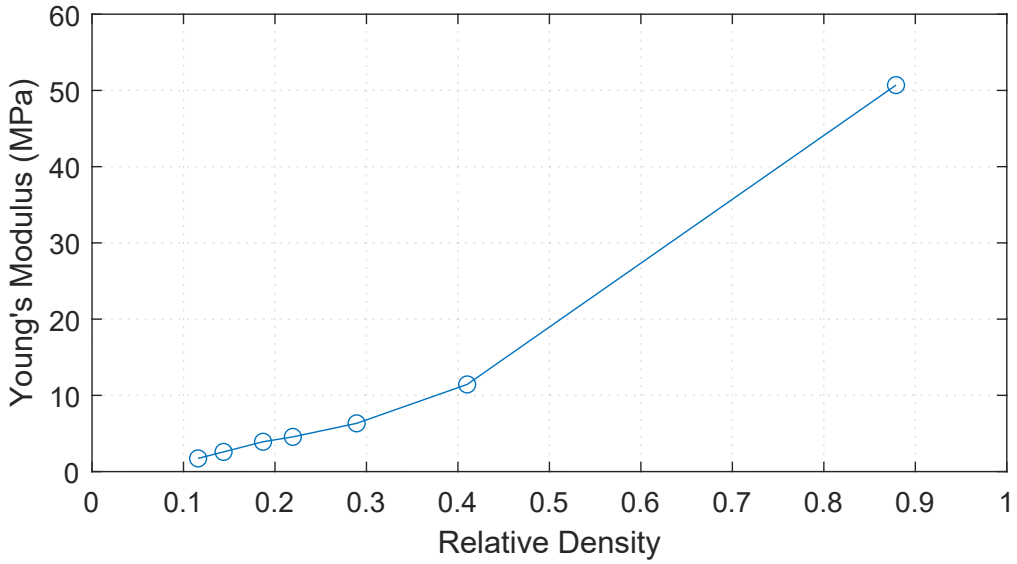

Figure 3.6: Extracted Young's Modulus vs. Relative density

Young's Modulus is a power function of the relative density. Since we have a lack of data between 0.4 and 0.88 and the real Young's Modulus of TPU is unknown, two interpolations have been proposed: one called 'Full Fit' which accounts for all the data and is also useful to estimate the Young's Modulus of TPU for later use in simulation software; the other instead interpolates only low density data and may be more precise on that interval. From the 'Full Fit' the Young's Modulus of TPU has been estimated to be $E_{TPU} = 64.1$MPa. The following proposed relations are characteristic of the *Gyroid* geometry and can be used to generalize

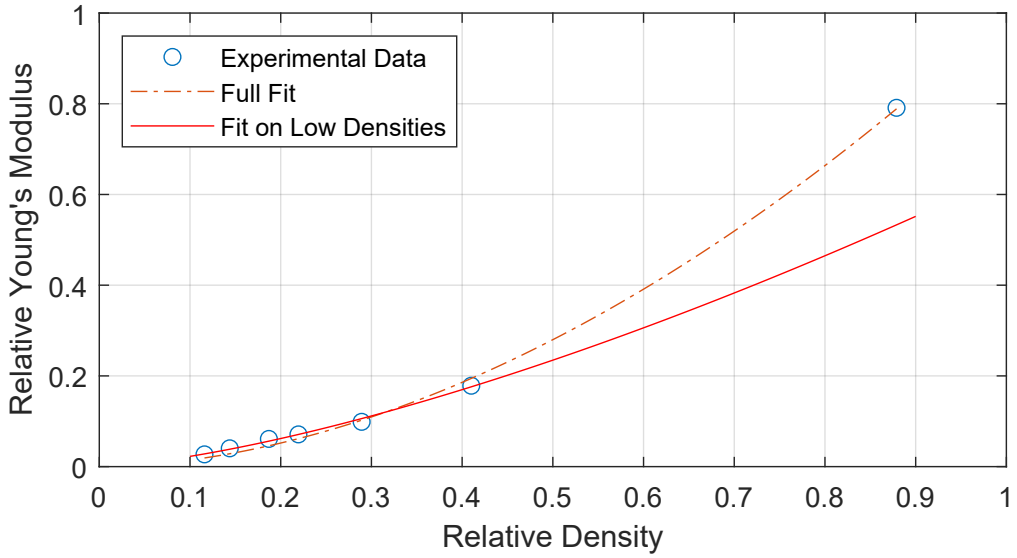

Figure 3.7: Two different Gibson Fit, one on full data and one restricted to low densities.

the behaviour (like equation 3.1) or to have a more accurate description around interval $\rho_r \in [0.1,0.4]$ density range.

$$\text{Full Gibson Fit:} \qquad E = E_{TPU} \cdot 0.99 \cdot \rho_r^{1.837} \tag{3.1}$$

$$\text{Local Fit:} \qquad E = E_{TPU} \cdot 0.643 \cdot \rho_r^{1.454} \tag{3.2}$$

From comparison with the theory of chapter 2 which predicts a trend ρ_r^2 the most reliable result is the Full Gibson Fit that shows an exponent b equal to 1.837.

3.4.3 Plateau Stresses

The linear interval of the compression curves starts to decline after a certain strain value and reaches a maximum peak when the first elastic collapse takes place. This statement is particularly true for low relative densities (<0.3) as predicted also by Gibson. This plateau is caused by an elastic buckling of the layers, when the *normal* stresses inside the walls leave place to pure *bending* behaviour. For higher densities a full plateau is not visible, mainly because the difference between normal and bending resistance starts to shrink, but still it is possible to note a decrease in $d\sigma/d\varepsilon$. In this case, the mean value of this pseudo-plateau will be taken as representative.

From the data in figure extrapolate a mathematical rule, two interpolations have been proposed: one linear and one with power function. Because we have only a limited set of data, both interpolation shows a coefficient of determination R^2 of

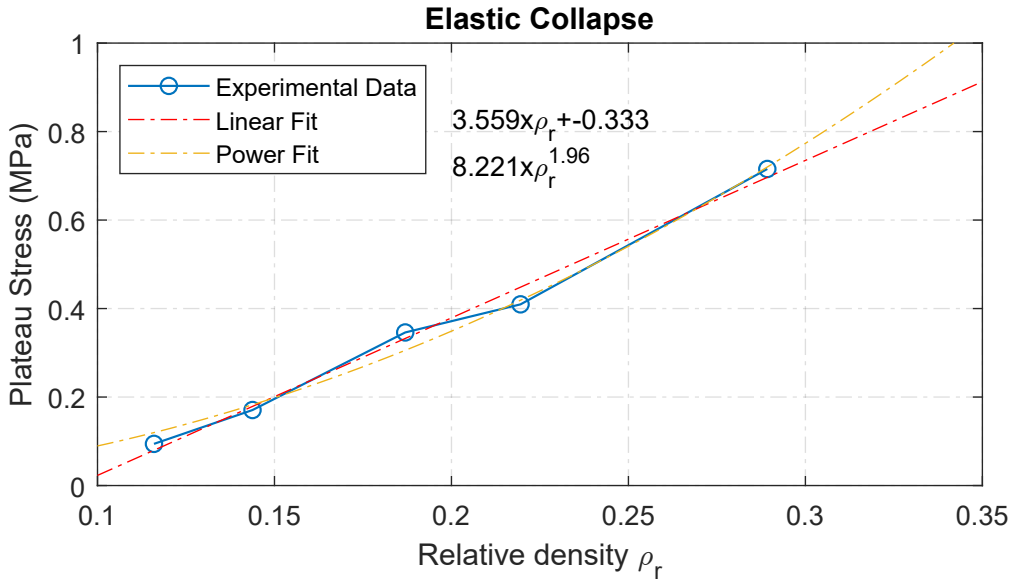

Figure 3.8: The lattice shows a constant stress over a major strain interval and depends on the relative density.

around 0.98, but since linear fitting predicts negative values for densities below 0.1, the Power Fit is preferred. The power coefficient of $1.96 \approx 2$ is compatible with the Gibson model which predicts $\sigma^*_{el} = C_4 \cdot \rho_r^2$, eventually multiplied by a corrective value.

3.4.4 Dynamic Behaviour

To characterize the transient behaviour of the TPU lattice, some cyclic loads have been applied.

The first test is conducted at a strain-rate of 10mm/min with the top limit at an absolute displacement of 20 mm and the bottom limit at a minimum force of 1N. After the first compression and crushing of the structure, the decompression shows a pronounced hysteresis cycle.

Referring to image 3.9, the total energy that is absorbed during one of the compression phases, calculated with numerical integration ($\int \sigma d\varepsilon$) is $830 J/m^2$ but only 52% of it is returned during the cycle. This value of energy return is quite low and can be useful or problematic, depending on the application.

Anyway, no significant plastic deformation happens inside the material, since few minutes after the removal of the load, the height returned to the original value within a tolerance of -0.3mm. This high-strain behaviour under compression load without permanent damage may be useful for applications where energy-absorption is required, for example on sport impact pads.

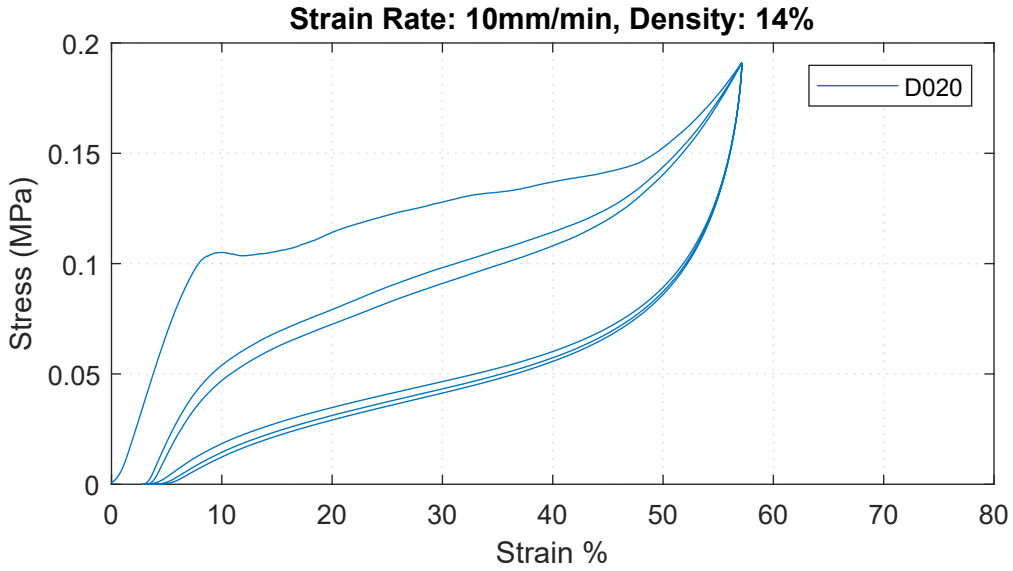

Figure 3.9

Since the target application is a sole or insole of shoe, it has been decided to simulate some realistic working conditions. A cyclic load in the range of $[1 \cdot 10^{-3}, 8 \cdot 10^{-2}]$MPa is *controlled by Force*, with a constant "Rate of Force Application". This means that the machine adds-up a certain amount of force every second. This condition seemed compatible with a walking foot, which every step loads the insole with full body-weight. Loads application rates were: -100N/s -50N/s -20N/s. Results are showed in figure 3.10.

The cycles occur across the elastic region and the energy return is around 80%, a value much higher than in the previous case, and much more suitable for footwear applications.

The same cyclic test has been performed on specimens with different densities with similar results (figure 3.11).

3.4.5 Anisotropic Behaviour

Fused Deposition Modelling is a process of addictive manufacturing, which means the volume is built by the addition of one layer at a time. So along the X and Y directions the material comes from a continuous flow of filament and is well bonded together, meanwhile the Z direction (the height) is comprised of multiple filament layers that mechanically adhere together when they are deposited at 210°C. This weakness in the bonding makes objects that are printed by FDM anisotropic in mechanical properties, particularly under tensile condition.

In our case, the main deformations inside the walls of the sheet-gyroid are

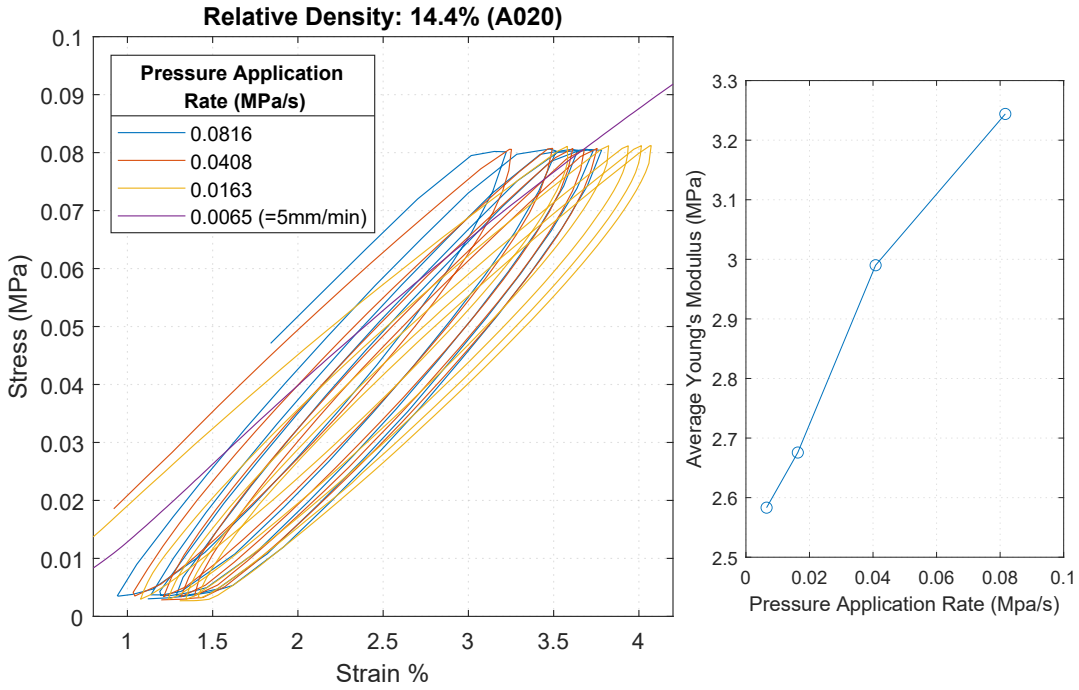

Figure 3.10: a) The hysteresis cycle changes shape at different force application rates. Static test on specimen A020 is added for comparison. b) The stiffness calculated from the average slope of the cycles.

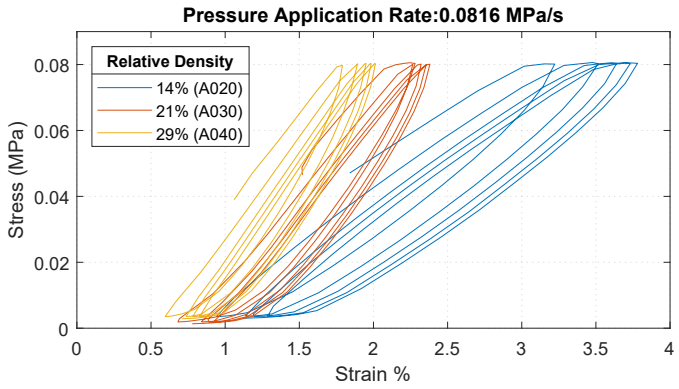

Figure 3.11: High-strain cyclic behaviour at different relative densities.

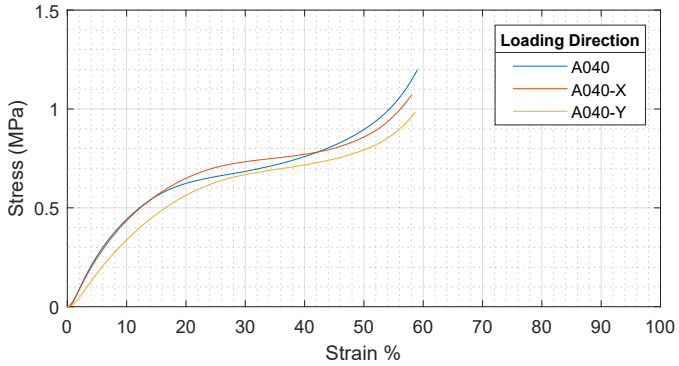

Figure 3.12: Comparison of compression along printing directions X,Y,Z.

bending and compression, but we tested the same specimen along the three principal direction to have a better insight. Figure 3.12 shows that there is a good match between the Z and X curves, but testing along the Y direction resulted in lower mechanical characteristics.

A possible explanation may lie in the amount of time passed between tests. In fact X was tested some minutes after Z, but Y was tested only few seconds after X. The residual elastic deformation (due to hysteresis) in the direction perpendicular to testing may have lowered the Young's Modulus of the specimen Y. Apart from speculations, the result is good.

3.5 Finite Element Analysis

Parallel to the experimental work, there is a work of prediction and simulation of the lattices with various approaches. Most of them relies on simulations by Finite Element Analysis and, if they are well refined can provide great insights in understanding how these geometries behave. [13]

3.5.1 Homogenization

One classic approach to simulate and make a rough estimation of the mechanical properties (i.e. stiffness) of cellular materials is to use *Homogenization*. This technique relies on simulating the response of the minimum repetitive geometry under different conditions to obtain a stiffness matrix. This matrix can be treated as a material itself and used in other simulations. From the practical point of view, the displacement of the nodes on opposites faces of the boundary box are fused together and the six fundamentals loads (3 axial, 3 shears) are applied.

The software nTop has a built-in tool to perform the homogenization, given any implicit body and a cell boundary region. In our case, the gyroid binary unit cell

is first generated from the scalar field. Then a tetrahedral solid mesh is generated from a surface mesh of the binary solid. This FE model is put together with basic material properties (E and ν) and the "Homogenize" tool automatically sets-up boundary conditions and loads. In output it is possible to visualize the directional stiffness as polar plot, to inspect how the material moves under the 6 fundamental loads and at the end to export the stiffness matrix in various formats ready for FEA software. Basic steps are shown in figure 3.13.

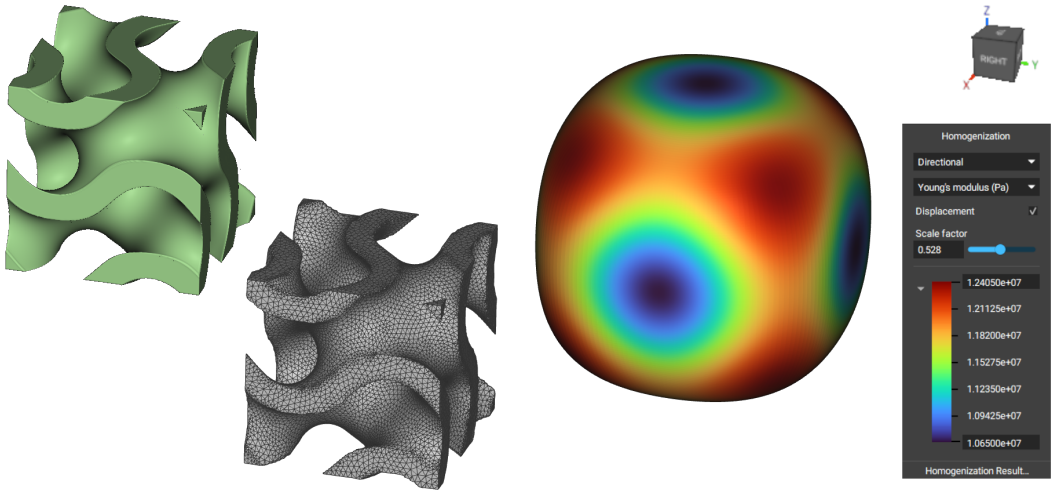

Figure 3.13

Homogenization has been performed at various densities and the output stiffness matrix exported in .csv. The base material Modulus used in simulation is $E = 64MPa$. This value has been inferred by the interpolation of experimental data with the 'Full Fit' ; The Poisson's ration is $\nu = 0.48$, extracted from generic material properties for TPU. The result of the homogenization is then imported into Matlab. From there, it's easy to extract the Young's Modulus. In fact:

$$[S] = [C]^{-}1$$

$$\frac{1}{E_{xx}} = S_{xx,xx}$$

where E_{xx} is the Young's Modulus along the direction xx (and for symmetry reasons Exx=Eyy=Ezz), $[C]$ is the stiffness matrix and $[S]$ is the compliance matrix, which is the inverse of the Stiffness matrix. The result has been plotted in graph 3.14 and overlapped with the experimental data and the 'Full Fit' power interpolation of the previous section.

Experimental data match extremely well with data extrapolated from Finite Element Analysis, while the interpolated trend shows a good fit, moving away from

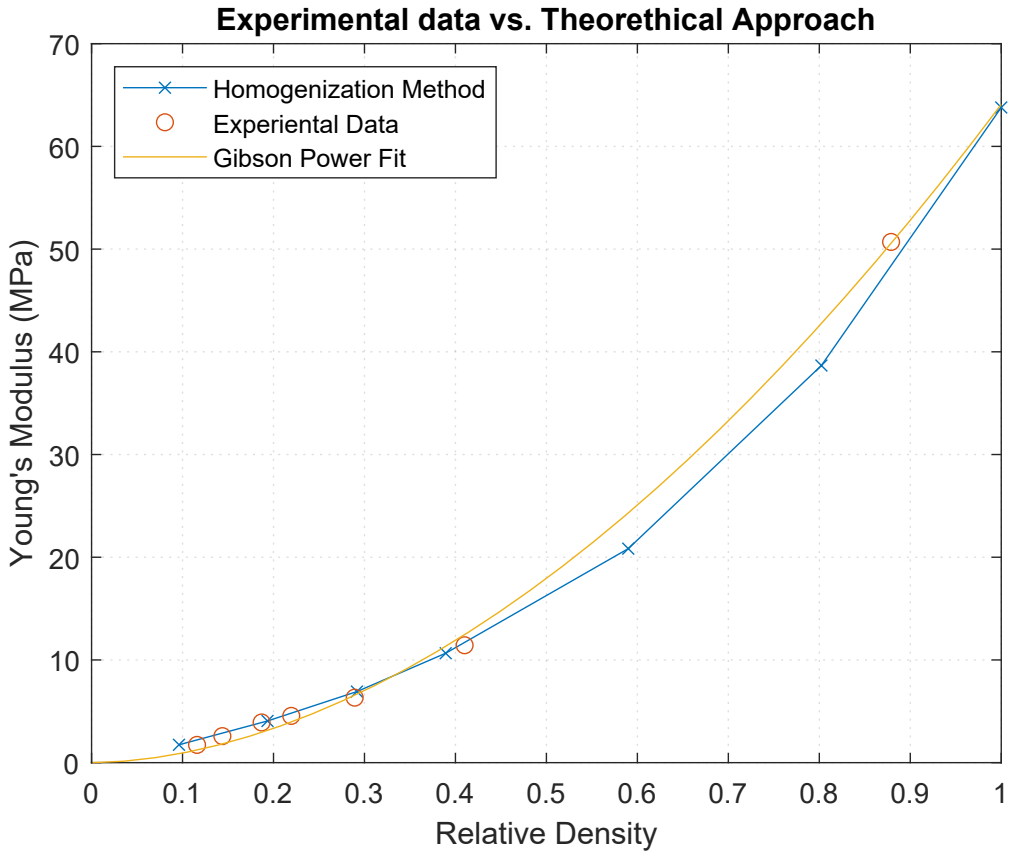

Figure 3.14: Comparison of results form Homogenization and experimental data (orange dots). Even without taking into account the edge effects, there is a great match between theory and specimens.

the FE results in the region $[0.4, 0.8]$ as a consequence of a lack of manufactured specimens in that area.

Even though the homogenization method is considered not suitable for a low number of unit cells, in our case of uniaxial load provided an accurate estimate of the linear behaviour of the lattice. This first approach will be adopted for sure in future to explore different lattice geometries.

3.5.2 Other Approaches

Finite Element Method can also be used in a multi-cell model, which represents the real lattice sample in the most accurate manner possible. The aim is to predict the behaviour in the most realistic load conditions, and a direct comparison with experimental results may be possible. The main difference with the homogenization is the modelling of the boundary conditions of the areas that are not periodic. For

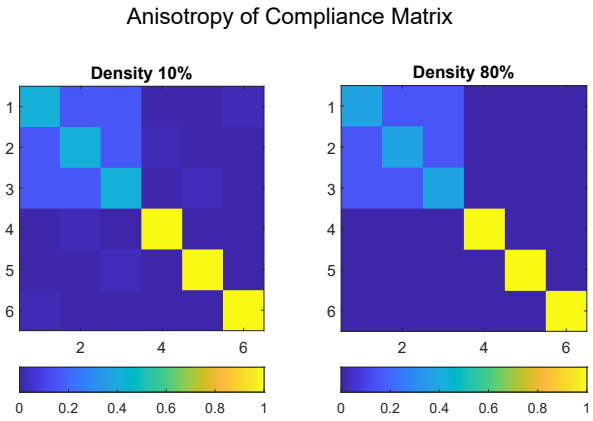

Figure 3.15: Visual display of compliance matrices. Although gyroid is quite orthotropic, at low densities it is possible to see some significant values on the Ist and IIIrd quadrants.

example the faces that are in contact with the universal testing machines have fixed displacement in the Z direction, and most probably also in the X ad Y directions (the friction between surfaces inhibits the movement). Also, the lateral faces are free can potentially behave differently to the rest of the sample and the distribution of the stresses can cause unexpected behaviour. This effect is also called *edge effect* and is relevant in trusses structures. Furthermore, the visual inspection of results

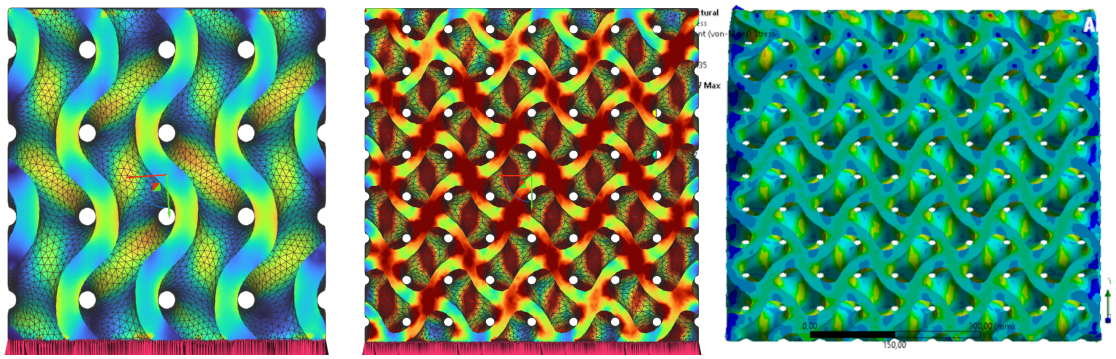

Figure 3.16: Sections views of the simulated samples. It's possible to see a small edge effect, but difficult to evaluate it's effect on the results.

from FE analysis can help to understand how the stresses are distributed inside the structure.

The analysis on gyroid stuctures, combined with the fit between the experimental data and the homogenization results, showed that the edge effect had only a weak

influence on the mechanical characteristics. Figure 3.16 shows that the edge effect is somehow visible, but not to a great extent. This is also due to the fact that the gyroid is geometrically made by distinct vertical walls (which are bended along a sinusoidal curve) (left in image) that connects to form horizontal layers at periodic heights (as center and right images show). Since the crushing of the failure is due to elastic buckling of these vertical walls, the stress σ^*_{el} is mostly influenced by the sectional area, and less influenced by some edge effects which are likely to occur on horizontal layers. A possible exception is when the boundary cube cuts one of these walls in half, a situation not occurred on our set of specimens and thus not analysed.

3.6 Architected Materials

In the previous sections we tested and analysed lattices with constant-density. This means that each specimen had a well defined ρ_r that remained constant across the volume. As seen, this type of lattices have a lot of properties in common with *foams* and cellular material descrybed by Gibson and Ashby in 1997[1].

Processes of making foams are various, ranging from mechanical to chemical to other sintering-like treatments. However, traditional foams usually are constant density, and the mechanical properties, that may vary at a microscopic level, are equally distributed across the volume at a macroscopic level.

One of the advantages of 3d-printing cellular structures is that it is possible to change and tune the geometry of the solid. This possibility expands the world of *architected metamaterials*: given a base material, it is possible to modify the geometrical characteristics of the lattice to obtain a desirable behaviour under a particular condition.

An example is the grading of the thickness of a lattice depending on the stress field calculated from Topology Optimization[14]. This enables to target the minimum required strength and reduce the overall weight of the component. Another example is to generate a lattice with a certain crushing plateau to limit the amount of pressure (during an impact: acceleration) and absorb the most amount of energy (an example is also provided in [1]).

An hypothesis is that by tuning the thickness, cell size and orientation it is possible to shape and control the Stress-Strain curve along its length. We tried to show how it is possible by referring to figure 3.18 which is the stress-strain curve of specimen 'RAMP'. In this specimen, the density increased linearly from the top to the bottom.

The curve does not behave like any other specimen. It does not present a significant decrease in stiffness that leads to the plateau phase. Instead it shows a quasi-linear behaviour along the whole curve, up to 50% strain where densification

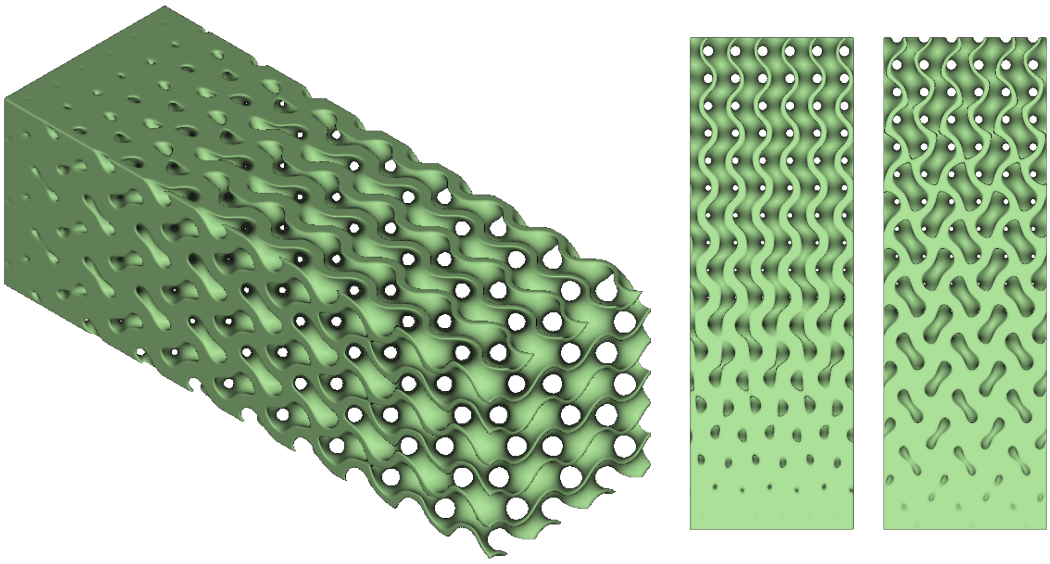

Figure 3.17: 'RAMP' specimen has a density that varies linearly between two opposite faces (direction z). As soon as the top layers enter the densification region, the lower layers enter the collapse region.

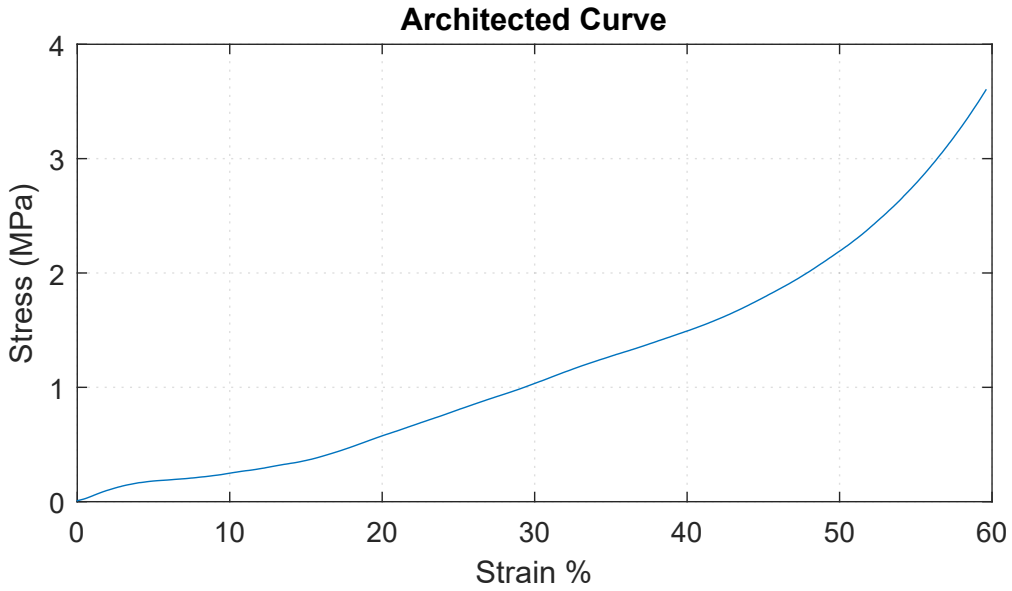

Figure 3.18

occurs. During testing, the first layers were soft and started to crush at around 5% total strain, but since their thickness was really limited to few millimeters, the

stress started to rise again. As soon as this happens, the second layer starts to reach it's plateau and balance the increase in stress. This layer-by-layer behaviour changes the response of the lattice in its full composition.

The same global phenomena was seen in Liu et Al. [15] but the material used was Ti-6Al-4V and it presented a full rupture of the layers. By using an elastomeric polymer there is no rupture and the transition is smooth.

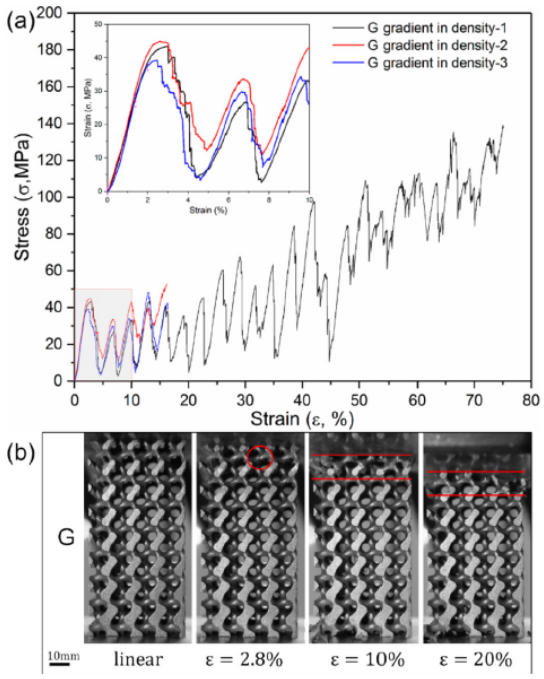

Figure 3.19: From Liu et Al. [15] shows a specimen with linear density ramp manufactured from Titanium. The material is quite brittle and fails layer by layer, bu it is possible to see how the stress-strain curve follows a linear trend.

Another example may be a lattice with two different densities along the compression direction z, stacked one on top of the other. After the less dense layer has reached densification, the curve becomes linear again until it reaches the second plateau. In this case we have architected a specimen which have two plateaus at different stress levels. We can for example build a component that is soft at touch but can provide protection during a hard impact, when the second plateau is activated.

We can try to model the compressive behaviour as a number of springs in series: the global compliance is the sum of the compliance of each spring. Each layer of the specimen has a different density that is function of the coordinate z, so a different local Young's modulus and SS curve. We can try to write the global Compliance

Modulus with a discrete approach or with a continuous approach:

$$\frac{1}{E_g} = C_g = \sum_{\text{Layers}} \frac{1}{E} \cdot H_{\text{layer}} = \int_z \frac{1}{E} \cdot dz \tag{3.3}$$

From section 3.4.2, the Young's Modulus is a function of the density as $E(\rho_r) = E_0 \cdot a \cdot \rho_r^b$. and $\rho_r = \rho_r(z)$. Equation can be rewritten:

$$C_g = \frac{1}{E_0 \cdot a} \int_z \rho_r(z)^{(-b)} dz \tag{3.4}$$

To solve the integral we must know how the density varies as a function of space. In our case 'RAMP' it was a linear function of the coordinate z such as $\rho_r(z) = m \cdot z + k$. Performing some substitutions leads to

$$\begin{aligned} dz &= d(\rho_r)/m \\ z &= (\rho_r - k)/m \end{aligned}$$

Defining the values for m and k by knowing the length of the piece and the range of densities inside the specimen (from design stage).

$$\begin{aligned} m &= (\rho_r^1 - \rho_r^0)/h \\ k &= (\rho_r^0) \end{aligned}$$

Solving the integral of equation 3.4 and substituting the relations from the previous formulae:

$$\begin{aligned} C_g &= \frac{1}{E_0 \cdot a} \frac{1}{m \cdot (1-b)} \Big[(m \cdot z + k)^{1-b} \Big]_0^h \\ C_g &= \frac{1}{E_0 \cdot a \cdot m \cdot (1-b)} \Big[(m \cdot h + k)^{1-b} - k^{1-b} \Big] \\ C_g &= \frac{1}{E_0 \cdot a \cdot (\rho_r^1 - \rho_r^0)/h \cdot (1-b)} \Big[((\rho_r^1 - \rho_r^0)/h \cdot h + \rho_r^0)^{1-b} - {\rho_r^0}^{1-b} \Big] \\ C_g &= \frac{1}{E_0 \cdot a \cdot (\rho_r^1 - \rho_r^0)/h \cdot (1-b)} \Big[{\rho_r^1}^{1-b} - {\rho_r^0}^{1-b} \Big] \end{aligned}$$

Of course C_g is the total compliance of the specimen and must be divided by the piece length to find the mean compliance of the material, useful to make a

comparison with available stiffness data.

$$C = \frac{C_g}{h} = 1/E_{ramp} \tag{3.5}$$

$$E_{ramp} = E_0 \cdot a \cdot \frac{h}{h} \cdot (1-b)\frac{(\rho_r^1 - \rho_r^0)}{(\rho_r^{1\,1-b} - \rho_r^{0\,1-b})} \tag{3.6}$$

$$E_{ramp} = 4{,}18\text{MPa} \tag{3.7}$$

$$\tag{3.8}$$

Solved for $a = 0.99, b = 1.837, \rho_r^1 = 0.1, \rho_r^0 = 0.5$ gives a value of $E_{ramp} = E_0 \cdot 0.0653 = 4{,}18$MPa. The value of linear stiffness extracted from experimental data is $= 4.03$MPa and confirms that our calculus is accurate.

This analytical expression is an example of how to proceed and is valid for this simple case, but for multidimensional and complex cases a numerical integration may be more suitable. It is also possible to expand this concept to non linear behaviour of the lattice, when the curves $\sigma = \sigma(\varepsilon)_{\rho_r}$ at various ρ_r values are known (from experimental curves or with an approximate model). We can also write:

$$\begin{cases} \delta_{tot} = \int \varepsilon dz & \text{total displacement} \\ \sigma_{tot} = \sigma_i & \text{stress is common} \end{cases} \tag{3.9}$$

In this case there is no direct way to find a solution, because function σ in general is not injective and $\varepsilon = \sigma^{-1}(\sigma)$ does not exist. So a method to approximate the solution in steps (just like non-linear FE solvers do) is required.

In conclusion, we have demonstrated experimentally that tuning the mechanical properties of lattice materials is possible and we tried to setup the basis for further analysis. The accuracy of 3d-printing technology opens up new possibilities in generating complex shapes, and thus manufacture advanced mechanical behaviours. Software that ease the design and simulation of lattice structures will play an important role in defining when and how this application will enter the consumer's markets.

Chapter 4

Case Study: Therapeutic Insoles

A orthoses is a medical device, customized on the patient, that has the function to compensate or correct a muscular, skelectric or postural disfunction. Insoles are orthotic devices that can have various purposes: antalgic, corrective and biomechanics.[16]

Antalgic insoles aim to reduce or remove pain from the foot region, caused by arthritis or inflammation, usually on elder patients. This insoles are usually soft to reduce impacts and distribute pressure evenly on the foot.

Corrective insoles are instead used in young patients to correct and guide the development of muscles and postural position. They are usually much stiffer, with thicknesses and hard supports.

Biomechanical insoles, the most complex to make, take into account the full movement of the feet during the walking cycle to compensate anomalies in "biomechanical" dynamics and in the natural equilibrium of the foot.

Orthopedic applications require a high level of customization, where the product is tailored around the body of the patient. Additive manufacturing offers a valid alternative to current manufacturing techniques. The traditional manufacturing processes include the casting of the foot and hand-processing or, alternatively, machine the desired shape with cnc from a full block of foam.

The advantages of using additive manufacturing (referring in particular to FDM) in a orthopedic laboratory can be several[17]:

- automated and linear production process;
- reduction in material waste;
- compact and clean workspace;

- materials already validated in the field;
- low investment budget.

Materials traditionally used are various, each with different material properties suitable for different cases. Common ones are cork, leather, thermoplastic materials, polymeric foams which can be modelled. External coatings are made of urethane polymers with open cells, which protect the skin tissue.[16]

Polyurethane (PU) is a polyester which can be solid or can be foamed. It is versatile and is used not only for insoles, but also for shoe soles and heels, thanks to its lightness and wear resistance [18].

The ability to tune mechanical characteristics such as stiffness and crushing behaviour by additive manufacturing opens a spectrum of possibilities for this material. In fact, buying a selection of materials and foams with different densities, where each must be processed with different technologies and expertise, is a labor intensive job and requires to master different abilities. The perspective of using the same material by tuning its characteristic it's a more standardized and linear process, and the automated manufacturing reduces the cost due to manual operations.

Some projects already specialized in the manufacturing of insoles for additive. In the Italian landscape *CreMED* (https://www.creamed.it) is teaming with medical professionals to make and test different insoles solutions. Another Italian startup sponsored also by European funds is *Medere* (https://medere.it), which also tune the infill of the insole to tune the cushioning. *Feetah* (https://feetah.it/) is an Italian project which is focused more on the software, and distribute a platform to create insole designs from 3d scans and digital streams of medical data. The digital model, suited to specific therapeutic needs under the guide of the specialist, can then be exported to a slicer software for 3d printing.

Our research belongs in this innovation field and expands the possibility of systematically and scientifically improving the performances and design of these products.

4.1 Design Workflow

The following workflow shows an example of how the previous knowledge and research can be applied to the production of a customized insole. The program used in this example is *nTopology*, because it's a commercially available software which naturally deals with implicit geometries and field manipulations. A custom code written, for example, in Matlab can provide a greater control over results and the possibility to build specific custom functions. Although, the concepts are the same so we provide the overview of the conceptual workflow.

1) The first step is to import into the software the data stream acquired by digital pressure measurements and 3d scan of the feet surface. The scan can be obtained by specific devices or from a sequence of images elaborated with a photogrammetry software. The model of the shoe can be also imported so to generate a product tailored not only on the patient's feet but also on the shape of the patient's shoes, maximising the wearability and the comfort.

The mesh models will be converted to Implicit Bodies, which allow to perform complex operations. Also, the pressure data, imported as point map in *.csv* format, is converted into a 2-d Scalar Field. This conversion enables to use the field values as an input to further calculations. This data will be the basis for the geometry generation and can be processed to target the required properties of the lattice structure to fill the geometry with.

2) A mathematical model or a series of experimental data is required to link the geometric features of lattices, such as density, to the mechanical behaviour that the final design will show. For example we can enter into the software the basic relations of stiffness over density and plateau stress over density, then reverse this relations. As seen in previous chapter, in the case of gyroid STPM made of TPU95A:

$$E = 64 \cdot \rho_r^{1.84} \qquad \rightarrow \qquad \rho_r = (E/64)^{(1/1.84)} \tag{4.1}$$

$$\sigma^*_{el} = 8.221 \cdot \rho_r^{1.96} \qquad \rightarrow \qquad \rho_r = (\sigma^*_{el}/8.221)^{(1/1.96)} \tag{4.2}$$

In this way we will be able to extract and apply the correct relative density. The designer will select one or both relations depending on the required mechanical properties of the application.

3) The third step is to generate the basic shape of the insole. this is the virtual equivalent to the physical molding process. One way to do it is to probe the profile of the foot at various heights with a plane created at the ground level and translated along Z axis. These profiles are then extruded up to another surface. It is possible to extrude up to ground level or up to the internal surface of the shoe. The shape will be generated as the union of the extruded profiles minus the shape of the foot (boolean difference). Since all the models are converted into implicit bodies, boolean operations will never fail.

4) Next, it may be necessary to customize the properties of the lattice and modify the shape generated at step 3. This part is strictly related on the therapeutic needs of the patient and is performed under the control of the therapeutic expert.

For example, let's take an insole with **Antalgic** function. This kind of device is essential for the treatment of diabetic foot, a severe condition where the patient

loses the skin perception in the foot area due to poor tissue oxygenation and blood circulation. The lack of feeling determines an unbalanced distribution of pressures on the ground, with high peaks in small areas. Skin tear apart and the foot ulcers may become infected. If not treated immediately this condition leads to necrosis and partial amputation of the limb.

For this reason it's extremely important to use preventive measures, which usually means redistributing the pressure across the foot. Lattice materials have a stress plateau that is function of the relative density. The plateau can be exploited to limit the effective pressure and redistribute it. In fact, as soon as one area reaches the threshold pressure, the lattice locally collapses, increasing contact over the boundary area and effectively limiting the maximum stress on the skin. This is the cushioning property of foams, and the same principle is already applied for bicycle and safety helmets, which must limit the acceleration exerted on the head during an impact. In fact foams of polystyrene and polyurethane are commonly selected and used in this field[1]. The difference is that by grading lattice it is possible to tune the plateau stress without having to change the material and buying the expanded foam with the correct density.

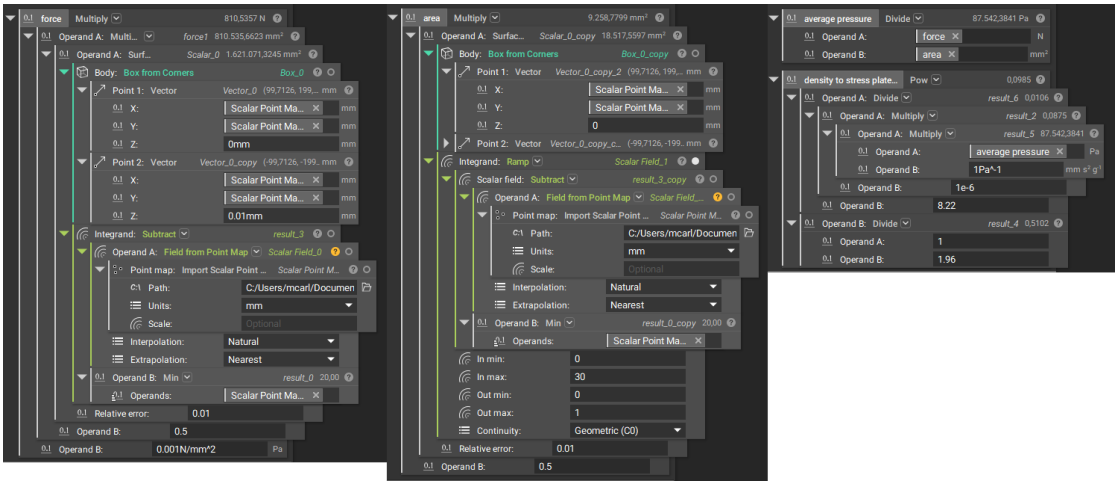

Figure 4.1: nTopology workflow. Surface integral is performed on the pressure field to calculate total weight and impression area. From this variables it's easy to figure out the required lattice thickness.

Starting from the scalar point pressure map converted into a planar scalar field, it is possible to integrate the pressure across the surface to calculate the total force due to weight and to integrate the contact points to extract the area of contact. The mean pressure, which represents the optimal pressure redistribution for a diabetic foot[16], is simply the ratio between force and area. Inserting this value

into the second equation of reference 4.1 will give the correct density for a lattice with a stress plateau equal to the mean pressure.

As seen in figure 4.1, in our example the weight on the foot is $81kg$, and the total contact area is $9200mm^2$, giving a target pressure of around $87kPa$. The required relative density for the gyroid lattice is $\rho_r = 9.8\%$.

5) Next step is to generate the theorized lattice with the field manipulation techniques explained in chapter 2. The lattice field is intersected with the solid from step 3. Other operations my be performed at this point:

- add of an external skin to prevent dirt inside the lattice geometry;
- cut out of a certain part not essential for the particular case (if the therapeutic action is limited to a certain area of the plantar surface);
- Arbitrary modification of thickness to increase or decrease support.

6) The final model is ready to be exported. At this point the implicit body has to be converted into a mesh. To accelerate and simplify the procedure, the implicit body is converted into a 3d binary matrix called *voxel matrix* because is composed by discrete cubic pixels (voxels). The resolution of the voxels must be high enough to capture all the details of the implicit body. The voxelized solid is then meshed into a triangular surface mesh, ready to be exported in the preferred format (.obj, .stl, .ply). This file can be opened by any slicing software and prepared for 3d printing.

If a MSLA technology is used instead of FDM, there is no need to create a mesh because the slices are sent to the printer as images. This task can be performed inside nTop platform from implicit bodies. This has the great advantage of saving computational effort, space on he hard drive and completely remove the slicing procedure.

4.2 Manufacturing Workflow

Once the model has been generated it must be manufactured. In this section we will show how it is possible to print the insole with a common FDM printer, a *Creality Ender 3*, using the software *Cura 4.8*. The insole generated from the previous section and shown in figure **??** will be used as the sample to be processed. The .obj mesh is imported into Cura and placed on the build plate. After selecting the material and the nozzle diameter preset it is possible to tune the printing parameters under print settings–>custom. In this case the options are the following:

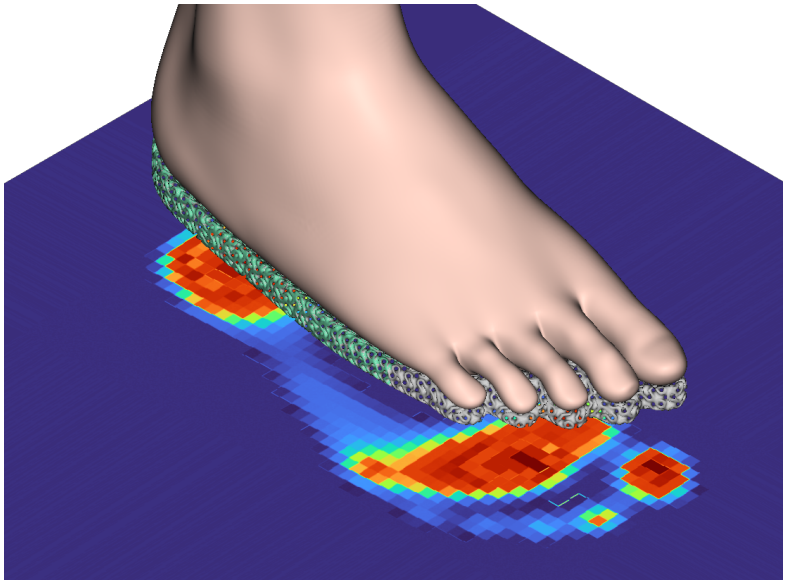

Figure 4.2: This image shows how the final insole is generated starting from biometric data and inherently tailored for the patient.

- line width=0.2 This value should be equal or grater to the nozzle diameter to provide adhesion between layers. It must be smaller than the smallest detail of the geometry. In our case the thickness of the walls is around 0.3 mm so a line width of 0.2 is recommended;
- layer height=0.12. The layer height must be smaller than the line width to guarantee good bonding between layers with a maximum recommended of 75% of line width. Moreover it must be smaller than the smallest detail of the geometry across the Z layer. On the opposite hand a value to small will inversely increase the printing time, so finding a compromise is important. To increase the movement precision it is possible to choose a so called "magic number", which is a multiple of the minimum movement provided by the sep-motor. A value of 0.12 satisfy all the needs;
- wall thickness=20. The model must be fully solid, so just select a number high enough o fill it completely. With the same purpose in mind bottom layers=999 and infill=100%.
- Compensate wall overlaps=on. To guarantee the correct size of thin walls this option must be activated together with minimum wall flow=0%;
- Printing temperature=210°C. This value is important for TPU and depends on the specific filament. From tests 210°C is enough to melt and guarantee a

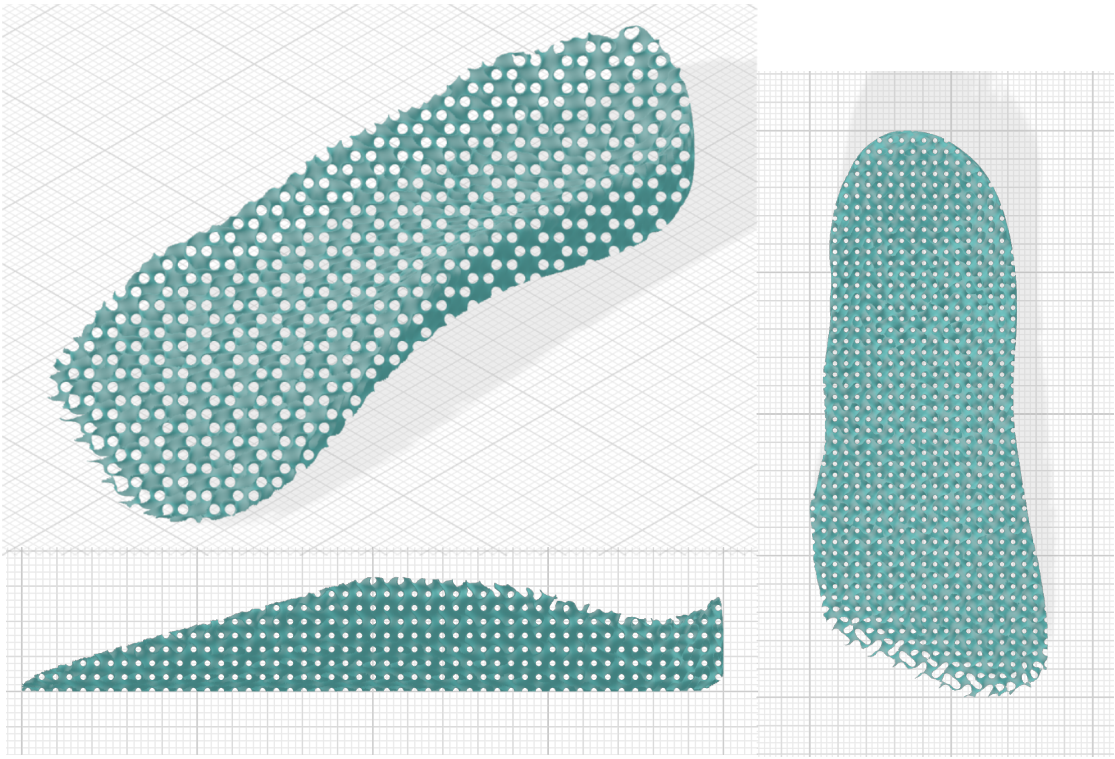

Figure 4.3: This image shows an insole engineered from practical example illustrated at step 4. The lattice density was designed to be 0.098. In our example, the dangerous peak of pressure was situated on the hill of the patient, so the insole was reduced in size with a cut in the middle to target specifically that area.

good adhesion but keep stringing effect under control. Stringing is when lines of plastic material are extruded mid-air while the hotend is moving between points. Plate temperature=off;

- Retraction=off. It depends on the printer. Retraction may reduce stringing but increase the printing time and for TPU is not recommended since the material is viscoelastic and generate a lag in the retraction action.

- print speed=[30-100]mm/s. Finding a good compromise between time and print quality is important. Gyroid is suitable to print at high speeds because the geometry does not have steep angles: in fact is also used as a standard infill in many slicing software with good results. The best results are when the speed is kept low by default and then tuned during printing directly from the machine. This allows to find the best compromise in real time.

The slicer generates the G-code, which is a file containing the instructions for the FDM printer, such as movements, speeds and extrusion rate. With the settings above, an insoles full of details requires around 12h of printing time. The material used is around 19g, which costs around 1€ (50€/kg) or 2€ for high quality material.

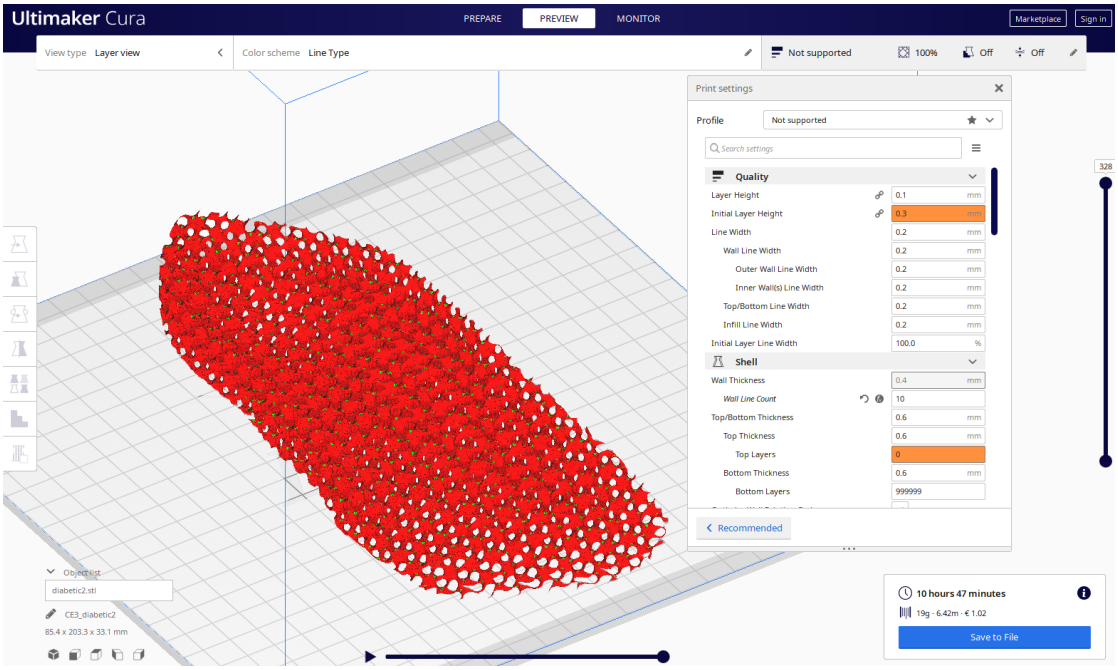

Figure 4.4: Cura 4.8 interface showing the insole for diabetic foot ready to be printed. On the right it's possible to control various parameters and after the slicing is done the software shows the estimated time and filament length.

The printing time may look high for a single piece but it must be considered that it is unsupervised work that completely substitute manual craftsmanship. The investment for a standard FDM printer can be less than 1000€ (as low as 200€ for the Ender 3) and estimating that the traditional molding and modelling of a insole device costs around 20€ in material and manual work, the initial investment is covered in a couple of months, conferring great potential to this new manufacturing technique. Moreover, some printers have a double symmetric extruder to print the symmetric insole (right and left) at the same time, effectively halving the time.

On a different design, which could be printed with a 0.6 mm nozzle, the printing time was as low as 3:40h. The final piece is shown in figure 4.5.

Figure 4.5: The prototype printed with a 0.3 mm nozzle in around 8 hours. A thin skin was added during design to increase comfort to the user, but trough the slice it's possible to see the lattice geometry.

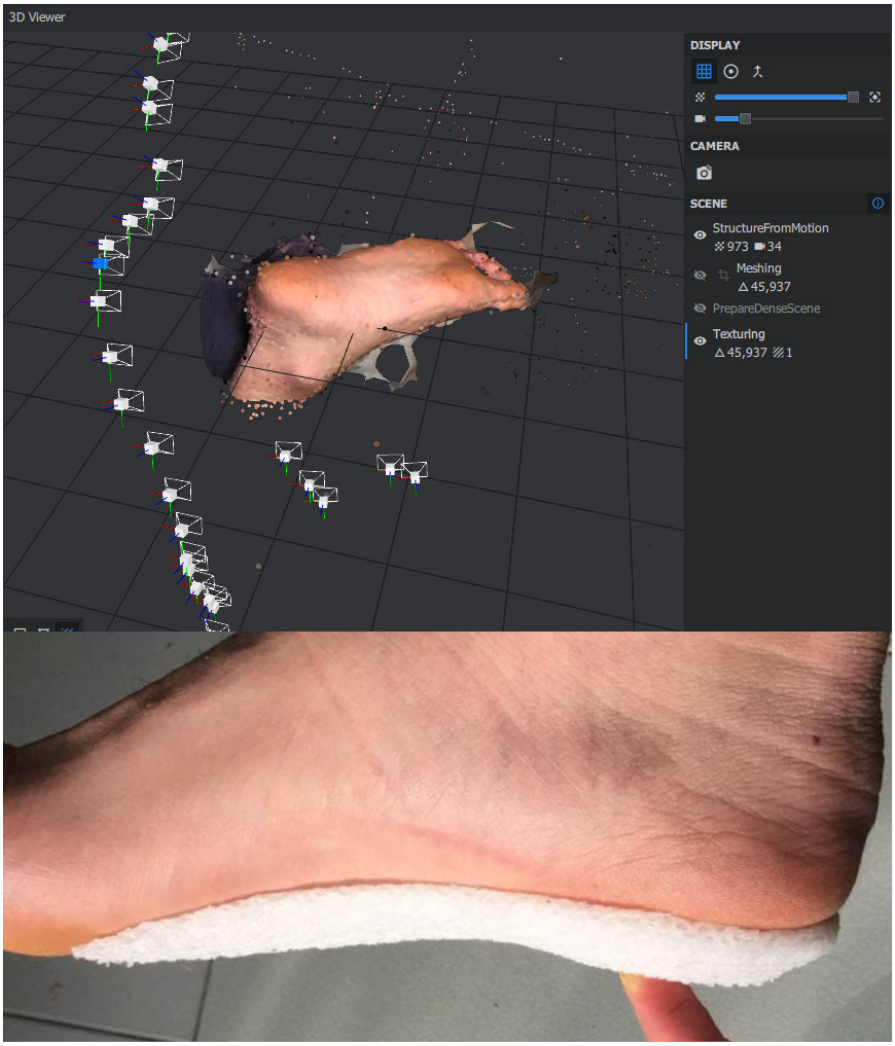

Figure 4.6: The photogrammetry used to extract the foot shape is meshroom and a video made with the camera of a cheap phone. The final insole shows a tight fit with the foot.

Chapter 5

Conclusions

The previous chapters presented the main concepts which gravitates around the design and manufacturing of Lattices, starting from the concepts of implicit bodies and field driven design and passing through material testing and simulation. The theory around cellular materials and foams has been developed by Gibson and Ashby since the 80's and by setting up a theoretical models that were able to predict the mechanical behaviour of such structures.

They showed that the deformation is driven by a combination of bending and stretching of microscopic elements. Under compression, a lattice follows a stress-strain curve with a linear trend, followed by a layer-by-layer crushing which establish a stress plateau. When full collapse occurs, a densification phase with high stiffness modulus takes place. This behaviour is typical of tough materials with plastic strains or elastomeric materials.

Altough the unit-cell topology is the fundamental parameter, also other parameters like the relative density plays a fundamental role in the mechanical properties of the lattice, which are predicted by various theoretical equations.

In the present work a particular topology has been chosen, a thin-walled structure generated by trigonometric functions, in particular the Gyroid which is part of the Triply Periodic Minimal Surfaces. Cubic samples with different relative densities ρ_r has been manufactured by Fused Deposition Modelling using TPU 95A, an elastomeric thermoplastic, as the base material. Compression tests at different strain rates and various load cycles were perfomed on samples, to study the influence on the behaviour and to tune the the theoretical models.

The results showed that the Young's Modulus of the geometry can be tuned in the range of $2 \div 60$MPa and the stress at the elastic collapse in a range of $0.1 \div 0.8$MPa. This ability is useful when designing cushions, energy absorbers, and anatomical applications.

A different approach based on Finite Element simulation has been taken into account. The technique called Homogenization is useful to extract the ideal

characteristics when he lattice is theoretically infinite. Even so, the results were so accurate that further analysis were considered unnecessary.

The aim of this work was to manufacture an orthopedic insole with the requested mechanical characteristics. In particular was designed an insole to relieve the pressure on the foot of a patient with diabetic foot to prevent injuries and ulcers.

Thanks to 3d-scanning, the insole is shaped on the patient's foot and eventually on the shoe shape to maximise comfort. Biometric data and pressures coming from baropodometric device are analyzed and used to tune the mechanical behaviour of the insole.

This technology recently raised a lot of interest because may reduce the amount of manual work and materials needed in manufacturing laboratory.

Bibliography

[1] Lorna J Gibson and M. F Ashby. *Cellular Solids: Structure and Properties*. 1997. URL: https://doi.org/10.1017/CBO9781139878326 (cit. on pp. 7, 19, 22, 27, 30, 38, 47, 55).

[2] *Mechanical testing and evaluation*. [11. ed.], 1. print. ASM handbook. ASM International, 2000. ISBN: 978-0-87170-389-7 (cit. on p. 9).

[3] «Selection and Industrial Applications of Hardness Tests». In: *Mechanical Testing and Evaluation*. ASM International, 2000, pp. 260–277. DOI: 10.31399/asm.hb.v08.a0003276. URL: https://dl.asminternational.org/books/book/47/chapter/536871/selection-and-industrial-applications-of-hardness (cit. on p. 9).

[4] URL: https://ntopology.com/ (cit. on p. 11).

[5] Antonio Gugliotta. *Elementi finiti*. Otto, 2002. ISBN: 9788887503456 (cit. on p. 13).

[6] Carlos M. Portela, Julia R. Greer, and Dennis M. Kochmann. «Impact of node geometry on the effective stiffness of non-slender three-dimensional truss lattice architectures». In: *Extreme Mechanics Letters* 22 (2018), pp. 138–148. DOI: 10.1016/j.eml.2018.06.004 (cit. on p. 15).

[7] I. J. Gibson and Michael Farries Ashby. «The mechanics of three-dimensional cellular materials». In: *Proceedings of the Royal Society of London. A. Mathematical and Physical Sciences* 382.1782 (1982), pp. 43–59. DOI: 10.1098/rspa.1982.0088 (cit. on pp. 18, 30).

[8] Oraib Alketan, Reza Rowshan, and Rashid Abu Al-Rub. «Topology-Mechanical Property Relationship of 3D Printed Strut, Skeletal, and Sheet Based Periodic Metallic Cellular Materials». In: *Additive Manufacturing* 19 (Jan. 2018), pp. 167–183. DOI: 10.1016/j.addma.2017.12.006 (cit. on pp. 18, 30, 37).

[9] URL: http://emlab.utep.edu/scSVL.htm (cit. on pp. 19, 23).

[10] S Teufelhart and G Reinhart. «Optimization of Strut Diameters in Lattice Structures». In: (), p. 15 (cit. on p. 23).

[11] *Cellular and Porous Materials in Structures and Processes*. CISM International Centre for Mechanical Sciences. Springer-Verlag, 2010. DOI: 10.1007/978-3-7091-0297-8. URL: https://www.springer.com/gp/book/9783709102961 (cit. on p. 31).

[12] URL: https://www.amazon.it/Filament-Flexible-3D-Dimensional-Accuracy/dp/B0863GRLLD/ (cit. on p. 34).

[13] Hanfeng Yin, Zhipeng Liu, Jinle Dai, Guilin Wen, and Chao Zhang. «Crushing behavior and optimization of sheet-based 3D periodic cellular structures». In: *Composites Part B: Engineering* 182 (Feb. 2020), p. 107565. DOI: 10.1016/j.compositesb.2019.107565 (cit. on p. 43).

[14] Ajit Panesar, Meisam Abdi, Duncan Hickman, and Ian Ashcroft. «Strategies for functionally graded lattice structures derived using topology optimisation for Additive Manufacturing». In: *Additive Manufacturing* 19 (Jan. 2018), pp. 81–94. DOI: 10.1016/j.addma.2017.11.008 (cit. on p. 47).

[15] Fei Liu, Zhongfa Mao, Peng Zhang, David Z. Zhang, Junjie Jiang, and Zhibo Ma. «Functionally graded porous scaffolds in multiple patterns: New design method, physical and mechanical properties». In: *Materials Design* 160 (Dec. 2018), pp. 849–860. DOI: 10.1016/j.matdes.2018.09.053 (cit. on p. 49).

[16] Eleonora Bonotto. «Analisi numerica dei fenomeni di interazione biomccanica piede-soletta». PhD thesis. Università degli studi di Padova, 2020. URL: http://tesi.cab.unipd.it/23488/1/BONOTTOELEONORABEATRICE_tesi.pdf (cit. on pp. 52, 53, 55).

[17] CreaMED. *[WEBINAR] [11-02-21] Flusso digitale in Podologia*. Feb. 2021. URL: https://www.youtube.com/watch?v=qUrwv6pEZ4Y&feature=youtu.be (cit. on p. 52).

[18] Anna Raumer. «Fenomeni di interazione piede-calzatura: caratterizzazione biomeccanica sperimentale e numerica». PhD thesis (cit. on p. 53).